Inorganic Chemistry

Article

pubs.acs.org/IC

Experimental and DFT Characterization of Metal-to-Ligand Charge-Transfer Excited States of (Rutheniumammine)(Monodentate Aromatic Ligand) Chromophores

Chia Nung Tsai,[†,‡] Yi-Han Tian,[†] Xuetao Shi,[‡] Richard L. Lord,[‡] H. Bernhard Schlegel,*[,‡] Yuan Jang Chen,*[,†,‡] and John F. Endicott*[,‡]

[†]Department of Chemistry, Fu-Jen Catholic University, New Taipei City 24205, Taiwan, Republic of China

[‡]Department of Chemistry, Wayne State University, Detroit, Michigan 48202, United States

Supporting Information

ABSTRACT: The heretofore unknown emission properties of the metal-to-ligand charge-transfer (MLCT) excited states of several complexes with (ruthenium)(monodentate aromatic ligand, MDA) chromophores are given. Emission spectra and lifetimes in 77 K glasses are reported for several monometallic complexes of the type $[Ru(NH_3)_{5-n}(L)_n(MDA)]^{2+}$ and two bimetallic pyrazine (pz)-bridged $[\{Ru(NH_3)_{4-n}(L)_n\}_2pz]^{4+}$ complexes (L = pz, pyridine, or a multipyridine ligand; MDA = pz or a substituted pyridine, Y-py). The emission maxima occur in the visible and near-IR spectral regions and have much more poorly resolved vibronic sidebands than do related complexes with Ru-bpy chromophores, and the excited-state lifetimes are characteristic of Ru-bpy MLCT excited states in this energy range. The emission yields of *trans*-$[Ru(NH_3)_4(MDA)(pz)]^{2+}$ (MDA = py or pz) are less than 0.2%, and combined with the other observations, this implies that most of the excited-state quenching occurs in high-energy excited states whose population precedes that of the lowest-energy ^{3}MLCT excited state. The pz-bridged, bimetallic complexes have mixed-valence excited states, and they absorb and emit at lower energies than their monometallic analogues do.

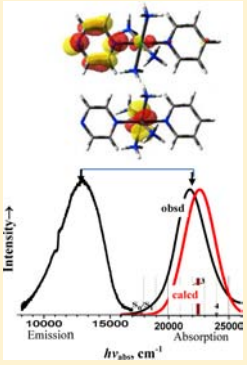

INTRODUCTION

Although the metal-to-ligand charge-transfer (MLCT) excited states of a very large number of ruthenium(II) complexes containing polydentate aromatic (bpy, tpy, etc.) ligands have well-characterized MLCT emission spectra,[1−5] the related emission properties of MLCT excited states of complexes with monodentate aromatic (MDA) ligands have not been previously reported. The emission from MLCT excited states of complexes with MDA ligands might be difficult to detect as a result of their unusually short lifetimes or unusual energies. There are many molecular properties that can affect the excited-state energies and lifetimes of these complexes, some of which have been well documented in the literature and others that have not.[6−14] The excited-state properties of complexes of the simple monobipyridine $[(L)_4Ru(bpy)]^{m+}$ complexes (L is a nominally "innocent" ligand) have been relatively well characterized,[15−21] and these complexes can provide a relatively straightforward basis for evaluating the MLCT excited-state properties of the related $[(L)_4Ru(MDA)_2]^{m+}$ complexes.

Among the factors that are important in determining the lifetimes of transition-metal MLCT excited states are (1) an ultrafast cascade from the initial Franck−Condon excited state to the lowest-energy MLCT excited state,[22] (2) the excited-state energies (the lifetime of the lowest-energy excited states of simple systems tends to increase with their energies),[23,24] (3) the differences in excited- and ground-state nuclear coordinates (the most distorted excited states tend to have shorter lifetimes),[20,21] (4) configurational mixing between low-energy MLCT excited states and their ground states (this tends to increase the energy differences and reduce the excited-state distortion, but the net effect is not well documented), (5) configurational mixing between the near in energy excited states of a complex (this can lead to excited-state potential energy surfaces with multiple minima and different distortions than might be expected),[18,21,25] and (6) lower-energy metal-centered (MC) excited states or thermally activated internal conversion to a low-energy triplet metal-centered excited state (^{3}MC) and other electronic states.[1,6−8,13,26,27] Figure 1 illustrates the simplest limit for which there is a single MLCT electronic configuration (and a possible MC excited state) but two MLCT states with different spin multiplicities.

Because the $[Ru(NH_3)_4(bpy)]^{2+}$ complex has a well-resolved 77 K emission spectrum,[16,17] it seems likely that the very closely related $[Ru(NH_3)_4(Y\text{-}py)_2]^{2+}$ complexes [Y-py is a substituted pyridine; Y = H, phenyl (ph), acetyl (ac), etc.] should also have reasonably well-defined MLCT excited states. Thus, the monodentate py ligands are relatively good σ donors,[28] and their bonding angles are not as constrained as those of the bpy ligand, so one would expect their complexes to have relatively high energy MC excited states. On the other hand, the lowest unoccupied molecular orbital (LUMO) of py is expected to be somewhat higher in energy than that of bpy, and the transfer of an electron to the acceptor should result in a

Received: February 22, 2013
Published: August 16, 2013

   dx.doi.org/10.1021/ic4016614 | *Inorg. Chem.* 2013, 52, 9774−9790

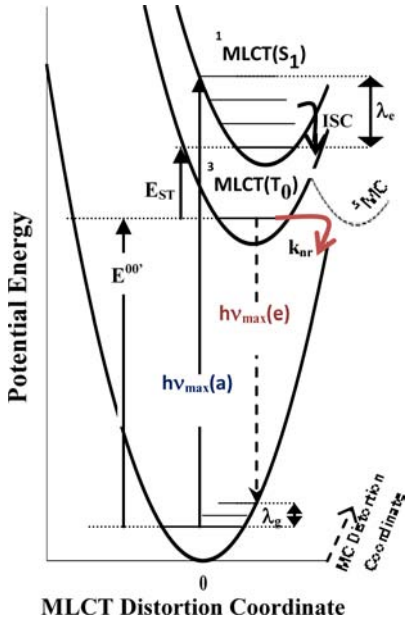

Figure 1. Qualitative potential energy curves for a $[(L)_4Ru(A)_2]^{m+}$ complex based on a single Ru^{II} and a single acceptor (A) orbital, which lead to a MLCT excited state with singlet or triplet spin multiplicity. A possible ^{3}MC is illustrated by the dashed curve. Note that the distortion coordinates for the ^{3}MC excited state are different from those for the MLCT excited states. The key parameters for discussing the excited-state properties are illustrated in the figure.

greater distortion of py than bpy because the distortions are expected to be distributed over more bonds in the latter. Consequently, it is surprising that there are, to our knowledge, no previous reports of the emission from MLCT excited states with MDA acceptor ligands.

In principle, excited-state energies and distortions can be inferred from emission spectra;[17,18,29−33] however, the excited-state distortions in such complexes are in a large number of vibrational modes,[15,17,34−36] which span the full range of metal/ligand ($h\nu_{vib}$ ~ 200−600 cm^{-1}) to internal acceptor ligand ($h\nu_{vib}$ ~ 1000−1600 cm^{-1}), and this greatly complicates the experimental determination of the excited-state energies and distortions from the typically broad band charge-transfer emission spectra that are found even in frozen solutions.[21,32,33]

The Ru^{II} center in these complexes has six electrons in nominally nonbonding orbitals and the monodentate py-like moieties would have one LUMO each so that there must be six times as many MLCT excited states as shown in Figure 1, and many of these excited states will differ little in energy. Consequently, the assignments of the absorption and emission spectra of these complexes and the evaluation of their excited-state distortions depend on high-quality computational modeling.[20,21]

We have found that several $[Ru(NH_3)_4(Y\text{-}py)_2]^{2+}$ and closely related $[Ru(NH_3)_4(L)pz]^{2+}$ complexes (pz = pyrazine) do have well-defined emission spectra. The $[Ru(NH_3)_4(L)pz]^{2+}$ complexes are of special interest because of their potential for constructing multimetal systems that can delocalize the electron density in their excited states.

EXPERIMENTAL SECTION

1. Materials and Synthesis of Compounds. Pyridine (py), ferrocene, trifluoromethanesulfonic acid (HOTF), 4-acetylpyridine (ac-py), 4-phenylpyridine (ph-py), pyrazine (pz), 2,2′-bipyridine (bpy), and 2,2′-bipyridylammine (bpyam) were purchased from Aldrich, and $[Ru(NH_3)_6]Cl_3$ and NH_4PF_6 were purchased from Strem Chemicals. These materials were used without further purification.

The syntheses of $[Ru(NH_3)_5Cl]Cl_2$, $[Ru(NH_3)_5(H_2O)](PF_6)_2$, *cis*-$[Ru(NH_3)_4(Cl)_2]Cl$, *trans*-$[Ru(NH_3)_4(L)(H_2O)](PF_6)_2$[37,38] (L = py, NH_3), and *mer*-$[Ru(NH_3)_3(bpy)(H_2O)](PF_6)_2$[37] were reported previously. Literature syntheses were used for the following compounds (numbers and letters are used in the figures below): $[Ru(NH_3)_5(L)]^{2+}$ complexes with L = py (**1**), ac-py (**2**), and pz (**3**),[7,39−41] *cis/trans*-$[Ru(NH_3)_4(L)_2](PF_6)_2$ with L = ac-py (**6c/6t**), ph-py (**5c/5t**), py (**4c/4t**), and pz (**7c/7t**),[20,36,42−44] and $[Ru(NH_3)_4(bpy)](PF_6)_2$ (**b**).[17] Variations in previously reported syntheses were used for the following compounds [see S1 in the Supporting Information for details; numbers and letters are used in the figures below]: $[Ru(NH_3)_5(pz)](ClO_4)_2$ (**3**),[40,41] *trans*-$[Ru(NH_3)_4(py)(pz)](BF_4)_2$ (**8**),[44] *mer*-$[Ru(NH_3)_3(bpy)(py)](PF_6)_2$ (**10**), *mer*-$[Ru(NH_3)_3(bpy)pz](PF_6)_2$ (**11**),[37,45] $[\{Ru(NH_3)_5\}_2(pz)](pz)](ClO_4)_4$ (**12**),[40,41] and *trans,trans*-$[\{Ru(NH_3)_4(py)\}_2(pz)](PF_6)_4$ (**13**).[37,46] All yields reported refer to isolated material judged to be homogeneous by NMR spectroscopy.

The skeletal structures of several of the ligands and their complexes are shown in Figure 2.

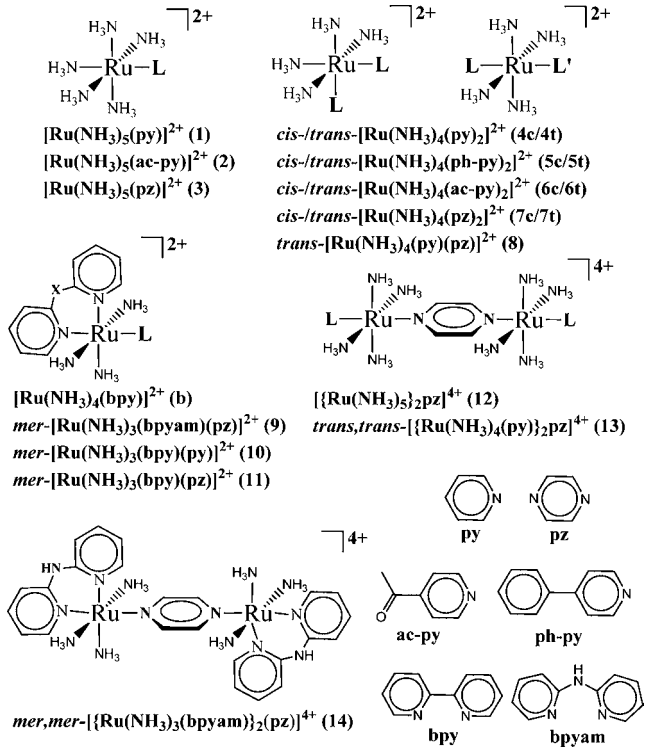

Figure 2. Skeletal structures of mono- and diruthenium complexes.

mer-[Ru(NH$_3$)$_3$(bpyam)(pz)](PF$_6$)$_2$ (9). The synthesis process of *mer*-$[Ru(NH_3)_3(bpyam)(H_2O)](PF_6)_2$ was based on a procedure reported for *mer*-$[Ru(NH_3)_3(bpy)(H_2O)](PF_6)_2$.[37] A sample of 200 mg of *mer*-$[Ru(NH_3)_3(bpyam)(H_2O)](PF_6)_2$ and a 10 mol excess of pz were added to 10 mL of a deaerated acetone/water mixture solution under argon, and the mixture was stirred for 3 h. Then, the red reaction mixture was filtered, and solid NH_4PF_6 was added until precipitation was completed, followed by cooling in an ice bath, and the resulting red product was removed by filtration. The product was washed with 1 mL of cold water followed by a second wash with 5 mL of cold ether. The product was dried in an oven under vacuum, and the typical yield was 20%. For **9**·2H_2O, anal./calcd for $C_{14}H_{26}N_8O_2P_2F_{12}Ru_1$: C, 23.05; N, 15.36; H, 3.59. Found: C, 23.32; N, 15.18; H, 3.33. ^{1}H NMR (acetone-d_6): δ 2.99 (br, 3H), 3.06 (br, 6H),

dx.doi.org/10.1021/ic4016614 | Inorg. Chem. 2013, 52, 9774−9790

6.93 (t, 1H), 7.18 (m, 2H), 7.30 (d, 1H), 7.74 (t, 1H), 7.85 (m, 2H), 8.48 (d, 2H), 8.62 (d, 1H), 8.84 (d, 2H), 9.51 (s, 1H).

*mer,mer-[{Ru(NH$_3$)$_3$(bpyam)}$_2$(pz)](PF$_6$)$_4$ (**14**).* A total of 15 mL of a degassed acetone solution containing *mer*-[Ru(NH$_3$)$_3$(bpyam)(H$_2$O)](PF$_6$)$_2$ (0.324 mmol) and **9** (0.27 mmol) was stirred for 14 h under argon. The blue-purple reaction mixture was filtered, and then 3 mL of water containing 3 g of NH_4PF_6 was added to an acetone solution, followed by cooling in an ice bath. The volume of the solution was reduced to 3 mL in the ice bath, and the purple precipitate was then removed by filtration. The product was washed with 1 mL of cold water followed by a second wash with 5 mL of cold ether. The product was dried in an oven under vacuum. For **14**·3H$_2$O, anal./calcd for $C_{24}H_{46}N_{14}O_3P_4F_{24}Ru_2$: C, 21.18; N, 14.41; H, 3.41. Found: C, 21.49; N, 14.01; H, 3.56. ^{1}H NMR (acetone-d_6): δ 2.91 (br, 18H), 6.98 (t, 2H), 7.17−7.18 (m, 4H), 7.32 (d, 2H), 7.77 (t, 2H), 7.88 (t, 2H), 8.02 (d, 2H), 8.60 (s, 4H), 8.63 (d, 2H), 9.58 (s, 2H).

2. Instrumentation. Emission spectra in 77 K glasses were obtained as described in detail elsewhere.[17,21,29] Spectra were calibrated for wavelength using xenon emission lines and for intensity using Oriel model 63358 quartz tungsten halogen (QTH) lamp. The emission spectra collected used (a) an ANDOR Shamrock 500 spectrometer with dual exit ports and equipped with three gratings: 150 l/mm, 800 nm blaze; 600 l/mm, 500 nm blaze; 300 l/mm, 1200 nm blaze. ANDOR Newton DU920-BV (for the visible range) and ANDOR iDus-InGaAs DU490A-1.7 [for the near-IR (NIR) range] detector heads were mounted on the exit ports of the Shamrock 500 spectrometer. The system was operated using ANDOR Solis spectroscopy software. The detector heads were cooled to −95 °C, and the spectrometer was purged with dry dinitrogen. The 77 K emission lifetimes were determined using a Spectra Physics 337205-00 nitrogen laser-pumped dye laser system for excitation and a Hamamatsu P9220 PMT/E717-63 socket assembly mounted on a Jobin-Yvon H-100 spectrometer for detection with the PMT output digitized using a PC containing a National Instruments NI PCI-5154, 2 GS/s, 1 GHz digitizer w/8 MB/ch onboard memory PC card.

Electrochemical measurements were performed using an Epsilon Electrochemical Workstation. Cyclic voltammograms (CV) and differential pulse voltammograms (DPV) were obtained in an acetonitrile solution, which contained a 10^{-3} M complex and 0.1 M *n*-tetrabutylammonium hexafluorophosphate (*n*-TBAH) at scan rates of 100 and 4 mV/s, respectively. A three-electrode system consisting of a platinum disk (1 mm) as the working electrode, polished with a 0.1−0.3 μm Baikowski alumina suspension, a platinum wire as the counter electrode, and Ag/AgCl as the reference electrode was used. Ferrocene (0.437 V vs Ag/AgCl in acetonitrile) was used as the internal standard. UV−visible−NIR absorption spectra in a solution of CH$_3$CN:H$_2$O = 1:1 (v/v) or pure acetonitrile were determined with a Shimadzu UV-3101PC spectrophotometer at 298 K. The spectral changes that accompanied redox titrations were obtained with the target complexes dissolved in the [DOTF] = 0.03 M solution [CH$_3$CN:D$_2$O = 1:1 (v/v)] and 3×10^{-3} M (NH$_3$)$_2$Ce(NO$_3$)$_6$, as the oxidant, or 1.5×10^{-3} M ferrocene, as the reductant; the CH$_3$CN:D$_2$O = 1:1 (v/v) solutions of both the oxidant and reductant contained 0.03 M DOTF.[47]

^{1}H and ^{13}C NMR spectra were obtained in acetone-d_6 on a Bruker Aspect-3000 (300 MHz) spectrometer.

3. Low-Temperature Absorption Spectra and Emission Yields. Absorption spectra in 87 K ethanol/methanol (4:1, v/v) glasses were obtained using calibrated xenon emission lines for wavelength and an Oriel model 63966 QTH lamp for intensity. The QTH lamp was also used as the light source in spectroscopic and yield measurements. A P/N 21530 Specac variable-temperature cell (−190 to +250 °C) with a square 1-cm-quartz cuvette as the controlled-temperature cell holder with liquid or glass samples was used. The detection system contained a motor-driven Jobin Yvon H-10 visible monochromator, a Hamamatsu R928 phototube with a Jobin-Yvon (JY) PMT-HVPS power supply, a JY Spectracq2 for data acquisition, and JY SynerJY software for data acquisition and data analysis. The Beer−Lambert law was used to calculate the absorbance (A) and molar absorptivity (ε)[48]

$$A = \log \frac{I_0}{I} = \varepsilon bc \tag{1}$$

where I_0 is the intensity of the incident light, I is the intensity of the transmitted light, b is the sample path length, and c is the substrate concentration.

The emission yields were based on spectra collected using an Horiba JY iHR 550 spectrometer with three gratings: 300 l/mm, 600 nm blaze; 300 l/mm, 1 μm blaze; 600 l/mm, 1 μm blaze. Horiba Symphony InGaAs-1700 (for the NIR range) detector heads were mounted on the exit ports of the iHR 550 spectrometer. The system was operated using SynerJY software. The detector heads were cooled to −90 °C, and the spectrometer was purged with dry dinitrogen.

[Os(bpy)$_3$]$^{2+}$ in 77 K ethanol/methanol glasses with a reference of the emission quantum yield of $\Phi_r \approx 0.038$[49] (λ_{max} = 435.8 nm excitation) was used as the reference for determination of the relative quantum yields for the complexes studied. Equation 1 was used to calculate the relative quantum yield of the target complex (Φ_{tc})[50]

$$\frac{\Phi_{tc}}{\Phi_r} = \frac{\eta_{tc}^2 I_{tc}}{\eta_r^2 I_r} \frac{1 - 10^{-A_r}}{1 - 10^{-A_{tc}}} \approx \frac{I_{tc} A_r}{I_r A_{tc}} \tag{2}$$

where I_{tc} and I_r are the integrated areas under the emission spectra of the targer complex and reference, respectively, A_{tc} and A_r are the absorbances of interest, respectively, η is the refractive index of the solvent, and $\eta_{tc}^2/\eta_r^2 = 1$ in the same solvent system. We used cylindrical 4-mm-id fluorescence cells immerseed in a Dewar with liquid nitrogen for the 77 K emission yield determinations. Because the sample path length, b in eq 1, is not well-defined for these cells and because the high concentrations are employed with very weakly emitting substrates (for absorbances of 2−5 in 1 cm), the yield determinations should be regarded as order of magnitude determinations.

Computational Details. Electronic structure calculations were carried out using density functional theory (DFT),[51] as implemented in a development version of Gaussian.[52] In a previous report of related Ru-bpy complexes,[20] we found that the B3PW91 functional[53−56] in combination with the SDDall basis set[56−59] correlated well with the experimental absorption spectra. In this report, we choose the SDD basis set, which employs the more flexible D95 V basis set for main-group atoms for a better description of the molecular geometries.[58] We have used both the B3PW91[53−56] and LC-wPBE[37,60,61] functionals to model the electronic structures of the complexes but find that the B3PW91 functional gives better agreement with the observed properties of the complexes.[20] Wave functions were tested for self-consistent-field (SCF) stability,[62,63] and all optimized structures were confirmed as minima by analyzing the harmonic vibrational frequencies.[64] Solvation effects (in acetonitrile) were accounted for using the most recent implementation of the implicit IEF-PCM solvation model.[65−68] Vertical electronic excitation energies and intensities were evaluated using time-dependent DFT (TD-DFT),[69−71] the orbital transitions of each excited state were characterized using the natural transition orbital (NTO) method,[52,72] and the isodensity plots of the orbitals involved in these transitions were visualized using *GaussView*.[73] The triplet MLCT excited states of *trans*-[Ru(NH$_3$)$_4$(py)(pz)]$^{2+}$ and *trans,trans*-[{Ru(NH$_3$)$_4$(py)}$_2$(pz)]$^{4+}$ were obtained using SCF calculations rather than TD-DFT. The calculation of the oxidation and reduction potentials of the complexes has been described previously[74] and used the B3PW91/SDD level of theory with zero-point-energy or thermal corrections; the present work did not include zero-point energies or thermal corrections. The calculated potentials were referenced to a calculated value of $E_{1/2}$ = 4.321 V for the AgCl/Ag couple under our level of theory.[75−77]

RESULTS

The experimental and computational parts of this study are complementary and have developed synergistically, but it is convenient to present some of the results separately.

dx.doi.org/10.1021/ic4016614 | Inorg. Chem. 2013, 52, 9774−9790

Table 1. Electrochemistry of Mono- and Diruthenium Complexes[a]

compd no.	complex	$E_{1/2}(Ru^{III/II})$	$E_{1/2}(L^{0/1-})$	$\Delta E_{1/2}(MV)^b$	$\Delta E_{1/2}(obsd)^c$	$\Delta E_{1/2}(calcd)^d$
1	$[Ru(NH_3)_5(py)]^{2+}$	0.419 (0.400)				3.18
2	$[Ru(NH_3)_5(ac\text{-}py)]^{2+}$	0.504 (0.488)				2.23
3	$[Ru(NH_3)_5(pz)]^{2+}$	0.591 (0.568)				2.84
4c	*cis*-$[Ru(NH_3)_4(py)_2]^{2+}$	0.631 (0.613)				3.22
4t	*trans*-$[Ru(NH_3)_4(py)_2]^{2+}$	0.595 (0.576)				3.03
5c	*cis*-$[Ru(NH_3)_4(ph\text{-}py)_2]^{2+}$	0.597 (0.569)				2.73
5t	*trans*-$[Ru(NH_3)_4(ph\text{-}py)_2]^{2+}$	0.588 (0.568)				2.58
6c	*cis*-$[Ru(NH_3)_4(ac\text{-}py)_2]^{2+}$	0.748 (0.727)				2.31
6t	*trans*-$[Ru(NH_3)_4(ac\text{-}py)_2]^{2+}$	0.730 (0.708)				2.15
7c	*cis*-$[Ru(NH_3)_4(pz)_2]^{2+}$	0.924 (0.906)				2.89
7t	*trans*-$[Ru(NH_3)_4(pz)_2]^{2+}$ [e]	0.901 (0.880)				2.65
8	*trans*-$[Ru(NH_3)_4(py)(pz)]^{2+}$	0.752 (0.732)				2.53
9	*mer*-$[Ru(NH_3)_3(bpyam)(pz)]^{2+}$	0.818 (0.792)				2.64
10	*mer*-$[Ru(NH_3)_3(bpy)(py)]^{2+}$	0.781 (0.764)	−1.566 (−1.524)		2.35	2.46
11	*mer*-$[Ru(NH_3)_3(bpy)(pz)]^{2+}$	0.905 (0.876)	−1.485 (−1.456)		2.39	2.44
12	$[\{Ru(NH_3)_5\}_2(pz)]^{4+}$	0.494 (0.468), 0.925 (0.904)		0.431		2.29
13	*trans,trans*-$[\{Ru(NH_3)_4(py)\}_2(pz)]^{4+}$	0.715 (0.692), 1.071 (1.048)		0.356		2.14
14	*mer,mer*-$[\{Ru(NH_3)_3(bpyam)\}_2(pz)]^{4+}$	0.767 (0.744), 1.118 (1.092)		0.351		2.11
b	$[Ru(NH_3)_4(bpy)]^{2+}$ [e]	0.61	−1.64		2.25	2.40

[a] $E_{1/2}$ values in CH_3CN/0.1 M *n*-TBAH vs Ag/AgCl at room temperature with a sweep rate of 0.1 V/s; DPV values in parentheses; referenced internally to $E_{1/2}(Fc^{+/0})$ = 0.437 V. [b] $E_{1/2(second)}(Ru^{III/II}) - E_{1/2(first)}(Ru^{III/II})$. [c] $E_{1/2(first)}(Ru^{III/II}) - E_{1/2}(L^{0/1-})$. [d] Difference between the calculated oxidation and reduction potentials; see Supporting Information Table S2.[45] [e] Reference 17.

Table 2. Ambient Absorption, 77 K Emission, and Lifetime Parameters of the Complexes[a]

compd no.	complex	$h\nu_{max}$(obsd),[b] $\times 10^3$ cm^{-1} (ε_{max}, $\times 10^3$ M^{-1} cm^{-1})	$h\nu_{max}$(emis),[c] $\times 10^3$ cm^{-1}	k_{obs}, μs^{-1} ($\tau_{1/2}$, μs)[d]
1	$[Ru(NH_3)_5(py)]^{2+}$	24.42 (7.5), 28.0 (2.9)		
2	$[Ru(NH_3)_5(ac\text{-}py)]^{2+}$	19.80 (11.9), 35.3 (2.7)		
3	$[Ru(NH_3)_5(pz)]^{2+}$	21.81 (11.9)		
4c	*cis*-$[Ru(NH_3)_4(py)_2]^{2+}$	23.65 (9.4), 26.84 (7.7)		
4t	*trans*-$[Ru(NH_3)_4(py)_2]^{2+}$	23.64 (16.48)		
5c	*cis*-$[Ru(NH_3)_4(ph\text{-}py)_2]^{2+}$	22.15 (19.8), 24.36 (16.4)[e]	14.8	0.31 (3.2)
5t	*trans*-$[Ru(NH_3)_4(ph\text{-}py)_2]^{2+}$	21.38 (26.9)[e]	14.63	0.25 (4.0)
6c	*cis*-$[Ru(NH_3)_4(ac\text{-}py)_2]^{2+}$	19.86 (15.8), 23.01 (11.1)[e]	12.62	6.7 (0.15)
6t	*trans*-$[Ru(NH_3)_4(ac\text{-}py)_2]^{2+}$	19.32 (23.9)[e]	11.94	9.4 (0.11)
7c	*cis*-$[Ru(NH_3)_4(pz)_2]^{2+}$	21.98 (12.9), 25.41 (9.6)	13.50	4.5 (0.22)
7t	*trans*-$[Ru(NH_3)_4(pz)_2]^{2+}$	21.34 (18.5)	14.22	2.0 (0.50)
8	*trans*-$[Ru(NH_3)_4(py)(pz)]^{2+}$	21.76 (17.5), 28.58 (2.3)	12.92	2.8 (0.35)
9	*mer*-$[Ru(NH_3)_3(bpyam)(pz)]^{2+}$	21.80 (13.1), 29.06 (3.4)	13.67	1.9 (0.53)
10	*mer*-$[Ru(NH_3)_3(bpy)(py)]^{2+}$	19.84 (7.11), 26.57 (11.9)	13.48	6.3 (0.16)
11	*mer*-$[Ru(NH_3)_3(bpy)(pz)]^{2+}$	20.17 (7.8), 24.57 (5.9)	13.98	4.9(0.21)
12	$[\{Ru(NH_3)_5\}_2(pz)]^{4+}$	18.32 (26.0)		
13	*trans,trans*-$[\{Ru(NH_3)_4(py)\}_2(pz)]^{4+}$	17.7 (38.5), 22.52 (3.0)	11.88	0.93 (1.1)
14	*mer,mer*-$[\{Ru(NH_3)_3(bpyam)\}_2\text{-}(pz)]^{4+}$	17.32 (37.9), 22.54 (4.6)	12.92	0.39 (2.6)
a	$[Ru(CH_3CN)_4(bpy)]^{2+}$ [f]	25.27	19.4	0.18 (5.5)
b	$[Ru(NH_3)_4(bpy)]^{2+}$ [f,g,h]	18.86 (4.0)	12.4	22 (0.045)
c	$[Ru(acac)_2(bpy)]$ [f]	16.10	10.8	

[a] Ambient absorption spectra were determined in acetonitrile or butyronitrile; emission spectra were determined at 77 K in butyronitrile glasses. [b] Low-energy absorption maxima. [c] Emission spectral maxima in 77 K butyronitrile glasses. [d] Mean excited-state decay lifetime. [e] Reference 20. [f] Reference 21. [g] Reference 17. [h] Reference 18.

A. Experimental Observations. In this study, we report the observed patterns of the absorption and emission spectra for several complexes with pz or substituted py chromophores. We have used DFT calculations to model the observed spectra, and because the DFT modeling indicates that the lowest-energy MLCT transition, S_0/S_1, in many of the complexes has a negligible oscillator strength, and because the ground-state reductions of the coordinated py and pz ligands were not often experimentally accessible, we have also used DFT calculations to demonstrate that the calculated S_0/S_1 transitions correlate as expected with the oxidation/reduction properties of the complexes.

The observed half-wave potentials of the complexes are shown in Table 1. The first electrochemical oxidation is attributed to the Ru centers, $E_{1/2}(Ru^{III/II})$, and the first reduction is attributed to the coordinated aromatic ligands, $E_{1/2}(L^{0/1-})$, of the complexes. The CV and DPV plots for these complexes are shown in the Supporting Information Figure S2.[45] The reductions of the Y-py and pz ligands of the monometallic complexes were out of the range of our

dx.doi.org/10.1021/ic4016614 | Inorg. Chem. 2013, 52, 9774−9790

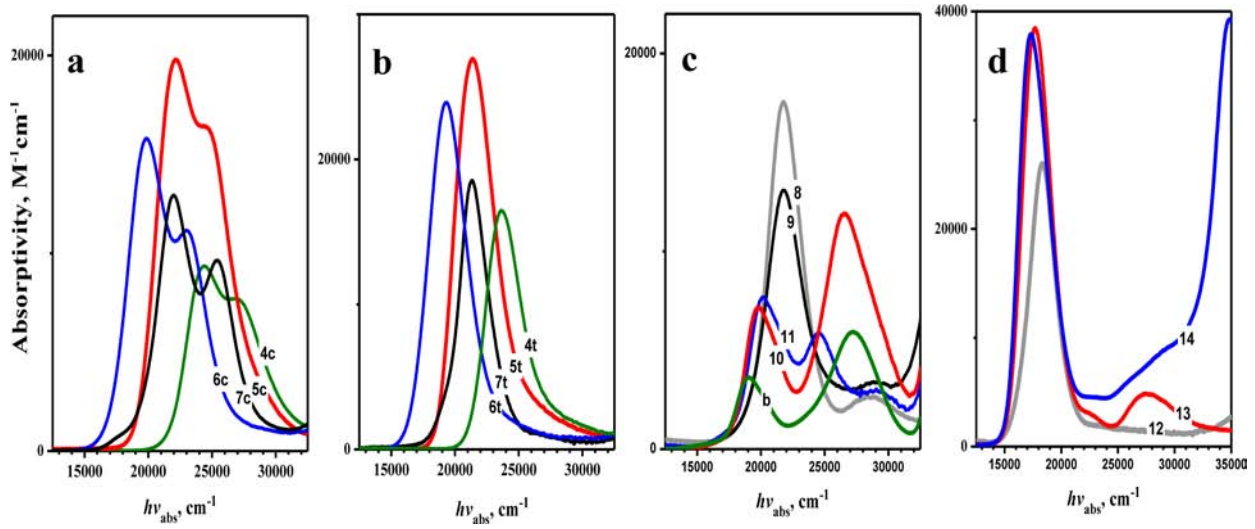

Figure 3. 298 K absorption spectra of the complexes: (a) *cis*-$[Ru(NH_3)_4(L)_2]^{2+}$ complexes with L = py (**4c**), phpy (**5c**), acpy (**6c**), and pz (**7c**); (b) *trans*-$[Ru(NH_3)_4(L)_2]^{2+}$ complexes with L = py (**4t**), phpy (**5t**), acpy (**6t**), and pz (**7t**); (c) *trans*-$[Ru(NH_3)_4(py)(pz)]^{2+}$ (**8**), $[Ru(NH_3)_4(bpy)]^{2+}$ (**b**), *mer*-$[Ru(NH_3)_3(bpyam)(pz)]^{2+}$ (**9**), *mer*-$[Ru(NH_3)_3(bpy)(py)]^{2+}$ (**10**), and *mer*-$[Ru(NH_3)_3(bpy)(pz)]^{2+}$ (**11**); (d) bimetallic complexes $[\{M\}_2(pz)]^{4+}$ with $\{M\} = \{Ru(NH_3)_5\}$ (**12**), *trans*-$\{Ru(NH_3)_4(py)\}$ (**13**), and *mer*-$\{Ru(NH_3)_3(bpyam)\}$ (**14**).

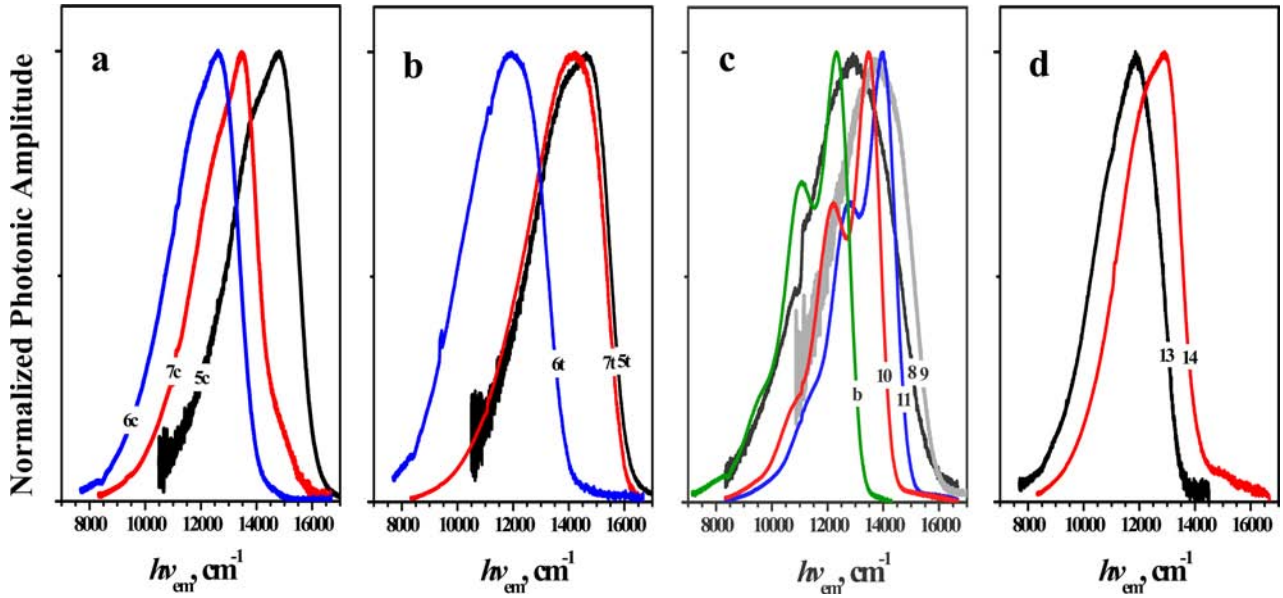

Figure 4. 77 K emission spectra of the complexes: (a) *cis*-$[Ru(NH_3)_4(L)_2]^{2+}$ complexes with L = phpy (**5c**), acpy (**6c**), and pz (**7c**); (b) *trans*-$[Ru(NH_3)_4(L)_2]^{2+}$ complexes with L = phpy (**5t**), acpy (**6t**), and pz (**7t**); (c) *trans*-$[Ru(NH_3)_4(py)(pz)]^{2+}$ (**8**), $[Ru(NH_3)_4(bpy)]^{2+}$ (**b**), and *mer*-$[Ru(NH_3)_3(LL)(L)]^{2+}$ with LL/L = bpyam/pz (**9**), bpy/py (**10**), and bpy/pz (**11**); (d) diruthenium complexes $[\{M\}_2(pz)]^{4+}$ with $\{M\}$ = *trans*-$\{Ru(NH_3)_4(py)\}$ (**13**) and *mer*-$\{Ru(NH_3)_3(bpyam)\}$ (**14**).

measurements. In view of the problems associated with the measurement of the monodentate ligand reduction potentials, we have calculated them; the calculated potentials are summarized in Supporting Information Table S2,[45] and the differences in the calculated oxidation and reduction potentials are reported in Table 1.

The ambient absorption parameters, 77 K emission spectra, and lifetimes of complexes are summarized in Table 2. The absorption spectra of mono- and diruthenium complexes in acetonitrile are shown in Figure 3. The ambient spectra of the *cis*-$[Ru(NH_3)_4(MDA)_2]^{2+}$ complexes exhibit two low-energy, intense MLCT absorption bands separated by about 3000–4000 cm^{-1}.[20,36] In contrast, the trans analogues have a single low-energy MLCT absorption that is more intense than either band of the cis complexes.

The 77 K emission spectra of several complexes are presented in Figure 4, and spectral and lifetime parameters are summarized in Table 2. The excited-state lifetimes of the $[(L)_4Ru(A)_2]^{m+}$ complexes at 77 K span a range of 0.11–4.0 μs (Table 2), which is very similar to that found for the MLCT excited states of the complexes $[(L)_4Ru(bpy)]^{2+}$. The observed 77 K Ru-L MLCT emission bands span the range of 10000–16000 cm^{-1}, which is also comparable the range observed for the $[(L)_4Ru(bpy)]^{2+}$ complexes, but the expected medium-frequency (ν_m = 1000–1600 cm^{-1}) vibronic sideband contributions that are attributable to distortions of the aromatic ligands are not resolved in the complexes with Ru-MDA

dx.doi.org/10.1021/ic4016614 | Inorg. Chem. 2013, 52, 9774–9790

Table 3. Summary of the Observed and Calculated Lowest-Energy MLCT Absorption Maxima for Some Mono- and Diruthenium Complexes

		MLCT absorption maxima, $\times 10^3$ cm^{-1} [a]		
		obsd	calcd[c]	
compd no.	complex	$h\nu_{max}$ ($h\nu_{lo}$) [$h\nu_{hi}$][b]	lowest-energy dominant[d]	S_0/S_1[e]
1	$[Ru(NH_3)_5(py)]^{2+}$	24.42 (21.2) [24.3]	25.7	20.8
2	$[Ru(NH_3)_5(ac\text{-}py)]^{2+}$	19.80 (15.6) [19.8]	21.3	15.0
3	$[Ru(NH_3)_5(pz)]^{2+}$	21.81 (18.0) [21.8]	25.3	17.6
4c	*cis*-$[Ru(NH_3)_4(py)_2]^{2+}$	24.38 (21.8) [24.1]	24.4	22.4
4t	*trans*-$[Ru(NH_3)_4(py)_2]^{2+}$	23.65 (21.6) [23.6]	22.9	21.1
5c	*cis*-$[Ru(NH_3)_4(ph\text{-}py)_2]^{2+h}$	22.15 (17.2) [21.9]	21.6	20.3
5t	*trans*-$[Ru(NH_3)_4(ph\text{-}py)_2]^{2+}$	21.38 (20.0) [21.4]	20.3	19.4
6c	*cis*-$[Ru(NH_3)_4(ac\text{-}py)_2]^{2+h}$	19.86 (16.5) [19.8]	19.3	17.2
6t	*trans*-$[Ru(NH_3)_4(ac\text{-}py)_2]^{2+}$	19.32 (15.6) [19.18]	17.9	15.8
7c	*cis*-$[Ru(NH_3)_4(pz)_2]^{2+}$	21.98 (18.34) [22.1]	23.1	20.2
7t	*trans*-$[Ru(NH_3)_4(pz)_2]^{2+}$	21.34 (16.7) [21.4]	21.4	17.6
8	*trans*-$[Ru(NH_3)_4(py)(pz)]^{2+}$	21.76 (17.7) [21.8]	22.6	17.9
9	*mer*-$[Ru(NH_3)_3(bpyam)(pz)]^{2+}$	21.80 (17.0) [21.8]	23.6	18.3
10	*mer*-$[Ru(NH_3)_3(bpy)(py)]^{2+}$	19.84 (16.3) [19.7]	20.8	16.4
11	*mer*-$[Ru(NH_3)_3(bpy)(pz)]^{2+}$	20.17 (16.6) [20.1]	21.5	17.6
12	$[\{Ru(NH_3)_5\}_2(pz)]^{4+}$	18.32 (16.1) [18.3]	21.2	16.2
13	*trans,trans*-$[\{Ru(NH_3)_4(py)\}_2(pz)]^{4+}$	17.71 (15.2) [17.4]	18.4	16.1
14	$[\{Ru(NH_3)_3(bpyam)\}_2(pz)]^{4+}$	17.3 (14.5) [17.1]	18.4	16.4
a	$[Ru(CH_3CN)_4(bpy)]^{2+}$	25.7	24.2	23.3
b	$[Ru(NH_3)_4(bpy)]^{2+}$ [e]	19	20.3	15.2
c	$[Ru(acac)_2(bpy)]$	16.1	18.2	12.9

[a]In acetonitrile. [b]$h\nu_{max}$ = lowest-energy observed MLCT band maximium; the $h\nu_{lo}$ and $h\nu_{hi}$ energy maxima are based on Gaussian deconvolutions of the absorption envelopes (see Supporting Information Figure S5).[45] [c]Vertical electronic energies and intensities based on the B3PW91 functional. [d]Energies based on the maxima of envelopes constructed by assigning a Gaussian of 2000−3000 cm^{-1} full-width at half-height to each calculated transition. [e]The lowest-energy calculated transition energy.

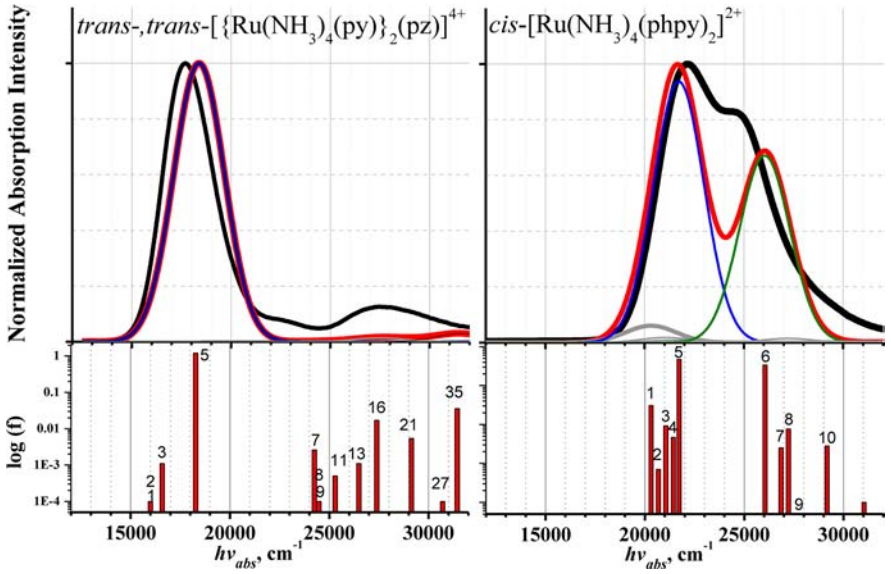

Figure 5. Comparison of the observed (black curves) and calculated (B3PW91; red curves) absorption envelopes for *trans,trans*-$[\{Ru(NH_3)_4(py)\}_2(pz)]^{4+}$, left panel, and *cis*-$[Ru(NH_3)_4(phpy)_2]^{2+}$, right panel. The calculated transitions and their calculated oscillator strengths (f) are numbered in order of increasing transition energy in the lower panels.

chromophores. These medium-frequency emission sidebands are only resolved for the monometallic complexes containing the bpy ligand (part c of Figure 4).

B. Observed and Calculated Absorption Spectra. Calculations based on the B3PW91 functional[53−56] for mono- and diruthenium complexes indicate that the ^{1}MLCT excited states whose transitions have the largest oscillator strengths appear to be 900−6300 and 2000−5000 cm^{-1}, respectively, higher than their lowest-energy charge-transfer excited states; see Table 3 and Supporting Information S6.[45] The spectra based on the B3PW91 functional are generally in good agreement with the observed spectra; see Figures 5 and 6. The calculations employing the LC-wPBE functional resulted in S_1 being a MC state for several complexes that exhibit strong

dx.doi.org/10.1021/ic4016614 | Inorg. Chem. 2013, 52, 9774−9790

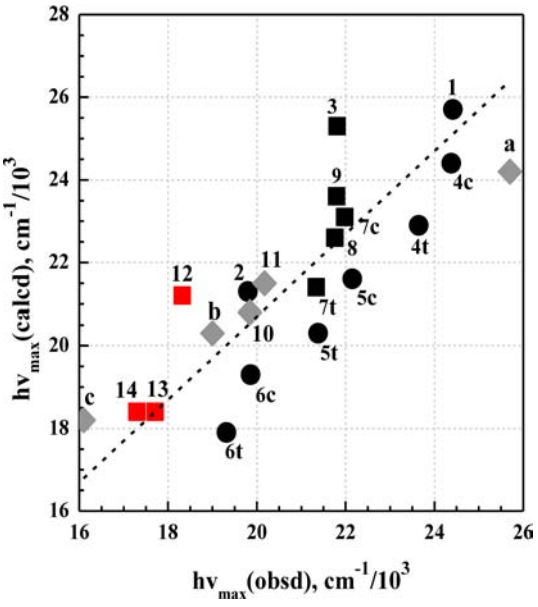

Figure 6. Correlation of the calculated (B3PW91) and observed MLCT absorption maxima of several complexes with Ru-A chromophores. The specific complexes related to the numbers and letters are identified in Table 2; squares for A = pz, black for monoruthenium complexes, and red for diruthenium complexes; circles for A = Y-py; diamonds for A = bpy. The dashed line is drawn with a slope of 1.00 and an intercept of 690 cm^{-1}.

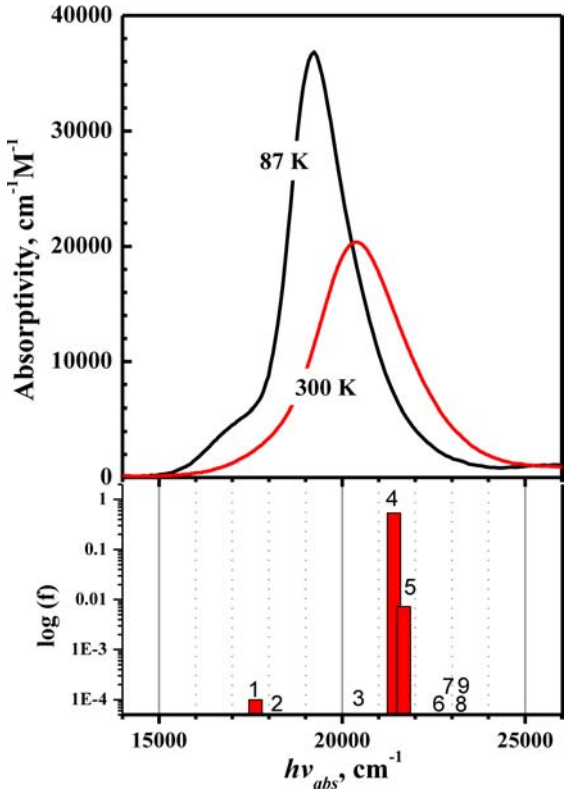

Figure 7. Comparison of the ambient and low-temperature absorption spectra of a *trans*-$[Ru(NH_3)_4(pz)_2]^{2+}$ complex in an ethanol/methanol solvent: solution at 300 K, red; glass at 87 K, black. The calculated transitions (numbered in the order of increasing energy) in the ground-state coordinates are shown in the bottom panel.

MLCT-like emissions (see Supporting Information S6).[45] This is possibly an artifact of the LC-wPBE functional and is being investigated.

The calculated NTOs[78,79] for the lowest-energy and dominant ^{1}MLCT excited states have different d-orbital compositions for these complexes, as illustrated in Supporting Information Figure S6.[45] Our calculations for the *mer*-$[Ru(NH_3)_3(bpy)(pz)]^{2+}$ complex indicate that its two lowest-energy ^{1}MLCT excited states, S_1 with the Ru-bpy chromophore and S_2 with the Ru-pz chromophore, are similar in energy, with the former lowest by less than 2000 cm^{-1}; see Supporting Information Figure S6.[45] The 77 K emission of this complex is consistent with this assignment because it exhibits the medium-frequency vibronic sideband that is characteristic of Ru-bpy chromophores.

Our computational modeling of the complexes and Ru-MDA chromophores has found that most of the lowest-energy transitions within the singlet manifold, involving the highest occupied molecular orbital (HOMO) and LUMO, have very small oscillator strengths. This is very similar to our observations on the complexes with Ru-bpy chromophores.[20] In most of the Ru-MDA complexes, these transitions appear as a low-energy tail of the dominant absorption band, and the interpretation of this is equivocal. At lower temperatures, the component bandwidths are appreciably decreased so low-temperature spectra should result in a better resolution of these weak transitions. We have determined the absorption spectrum of *trans*-$[Ru(NH_3)_4(pz)_2]^{2+}$ at 87 K (Figure 7), and the weak transition appears as a well-defined absorption shoulder, providing further experimental support for this aspect of the modeling. The calculated energy difference between the dominant transition (Supporting Information S4) and the S_0/S_1 transition is 3800 cm^{-1}, while the energy difference between the 87 K absorption maximum and low-energy shoulder is 2200 cm^{-1}.

C. Observed Emission Spectra and Computational Modeling of Triplet States. The 77 K emission maxima of the pz-bridged *trans,trans*-$[\{Ru(NH_3)_4(py)\}_2pz]^{4+}$ and *mer,mer*-$[\{Ru(NH_3)_3(bpyam)\}_2(pz)]^{4+}$ (see Figure 4 and Table 2) are about 1000 and 750 cm^{-1} lower in energy than their monometallic analogues but with typically smaller overall spectral widths and no resolved vibronic sidebands. This is illustrated in Figure 4 for the *trans*-$[Ru(NH_3)_4(py)(pz)]^{2+}$ and *trans,trans*-$[\{Ru(NH_3)_4(py)\}_2pz]^{4+}$ complexes; the emission lifetimes for these two complexes are 0.35 and 1.1 μs, respectively, in the butyronitrile glasses. The two equivalent metal centers of the ground-state bimetallic complexes $[\{Ru(NH_3)_5\}_2pz]^{4+}$, *trans,trans*-$[\{Ru(NH_3)_4(py)\}_2(pz)]^{4+}$, and *mer,mer*-$[\{Ru(NH_3)_3(bpyam)\}_2(pz)]^{4+}$ are oxidized at potentials differing by 0.431, 0.356, and 0.351 V ($\Delta E_{1/2}$; see Table 1), respectively, and their one-electron oxidations result in intense $Ru^{III/II}$ mixed-valence absorption bands at about 6000 cm^{-1} (see Supporting Information Figure S3)[45] typical of this class of complexes.[40,41]

We obtained emission quantum yields of 0.00005 and 0.00004, respectively, for *trans*-$[Ru(NH_3)_4(pz)_2]^{2+}$ and *trans*-$[Ru(NH_3)_4(pz)(py)]^{2+}$ in 4:1 ethanol/methanol glasses at 77 K. The 77 K emission yields for these complexes are 4−30 times larger in butyronitrile (Table 6).

We have modeled the triplet as well as singlet excited-state manifolds of several of the complexes, and the overall modeling results are summarized in Table 4.

dx.doi.org/10.1021/ic4016614 | Inorg. Chem. 2013, 52, 9774−9790

Table 4. Comparison of the Calculated Excited-State Transition Energies for Singlet and Triplet MLCT Excited States Evaluated in the Nuclear Coordinates of the Ground State (S_0) and Lowest-Energy MLCT Excited State (T_0)

complex (compd no)	approximate SOMO occupation of the excited state[a]	excited-state transition energies in the coordinates of the S_0 minimum, $\times10^3$ cm^{-1}		λ_g[b] (SCF)	excited-state transition energies in the coordinates of the T_0 minimum, $\times10^3$ cm^{-1}		$h\nu_{max}$(obsd) ($h\nu_{max}$(emis)), $\times10^3$ cm^{-1}
		singlet	triplet		singlet	triplet	
$[Ru(NH_3)_5(pz)]^{2+}$ (3)	$d_{xy} \rightarrow pz$	17.6 (S_1)	16.3 (T_1)	4.1	13.2 (S_1)	11.4 (T_1)	
	$d_{xz} \rightarrow pz$	18.0 (S_2)	16.5 (T_2)		13.5 (S_2)	11.5 (T_2)	
	$d_{yz} \rightarrow pz$	25.2 (S_3) (dominant)	13.1 (T_0)		18.6 (S_3) (dominant)	6.8 (T_0)	
$[Ru(NH_3)_5(py)]^{2+}$ (1)	$d_{xy} \rightarrow py$	20.8 (S_1)	20.0 (T_1)	5.8	14.7 (S_2)	12.7 (T_2)	
	$d_{xz} \rightarrow py$	21.1 (S_2)	20.1 (T_2)		14.6 (S_1)	12.6 (T_1)	
	$d_{yz} \rightarrow py$	25.7 (S_3) (dominant)	16.8 (T_0)		16.4 (S_3) (dominant)	8.5 (T_0)	
trans-$[Ru(NH_3)_4(py)(pz)]^{2+}$ (8)	$d_{xy} \rightarrow pz$	17.9 (S_1)	17.1 (T_1)	3.8	13.9 (S_1)	12.3 (T_1)	
	$d_{xz} \rightarrow pz$	18.6 (S_2)	17.7 (T_2)		14.5 (S_2)	12.8 (T_2)	
	$d_{yz} \rightarrow pz$	22.6 (S_3) (dominant)	14.5 (T_0)		17.9 (S_3) (dominant)	8.5 (T_0)	12.9 (12.3)
trans-$[Ru(NH_3)_4(pz)_2]^{2+}$ (7t)	$d_{xy} \rightarrow pz$	17.7 (S_1), 20.6 (S_3)	17.6 (T_2)	4.3	14.3 (S_1)	13.0 (T_1)	
	$d_{xz} \rightarrow pz$	18.4 (S_2)	18.3 (T_3)		15.1 (S_2)	13.6 (T_2)	
	$d_{yz} \rightarrow pz$	21.5 (S_4) (dominant)	16.1 (T_0), 17.1 (T_1)		17.5 (S_3) (dominant)	10.0 (T_0)	13.5 (14.3)
trans-$[Ru(NH_3)_4(py)_2]^{2+}$ (4t)	$d_{xy} \rightarrow py$	21.1 (S_1)	21.1 (T_2)	6.0	15.6 (S_1)	13.9 (T_1)	
	$d_{xz} \rightarrow py$	21.5 (S_2)	21.5 (T_3)		16.0 (S_2)	14.2 (T_2)	
	$d_{yz} \rightarrow py$	22.9 (S_3) (dominant)	18.3 (T_0)		16.3 (S_3) (dominant)	10.3 (T_0)	
trans,trans-$[\{Ru(NH_3)_4(py)\}_2(pz)]^{4+}$ (13)	d_{xy}-$d_{xy} \rightarrow pz$	16.1 (S_1)	15.2 (T_1)	1.0	15.1 (S_1)	14.0 (T_1)	
	$d_{xy} + d_{xy} \rightarrow pz$	16.1 (S_2)	15.2 (T_2)		15.1 (S_2)	14.0 (T_2)	
	$d_{xz} - d_{xz} \rightarrow pz$	16.7 (S_3)	15.6 (T_4)		15.8 (S_3)	14.4 (T_4)	
	$d_{xz} + d_{xz} \rightarrow pz$	17.1 (S_4)	16.0 (T_5)		16.1 (S_4)	14.8 (T_5)	
	$d_{yz} - d_{yz} \rightarrow pz$	18.4 (S_5) (dominant)	10.3 (T_0)		18.0 (S_5)	7.9 (T_0)	11.9 (8.9)
	$d_{yz} + d_{yz} \rightarrow pz$	24.2 (S_6)	15.3 (T_3)		24.4 (S_6)	14.2 (T_3)	

[a]Cartesian coordinates defined with respect to the plane of the MDA ring. [b]See Figure 1.

We have also calculated the lowest-energy ^{3}MC excited-state energies for *trans*-$[Ru(NH_3)_4(pz)_2]^{2+}$, and the details for the former are summarized in Table 5. In Table 5, the singly occupied orbitals are expressed in terms of corresponding orbital plots; the corresponding orbital is very similar to the NTO and is a transformation such that the triplet spin contributions are almost entirely from α-HOMO and α-HOMO−1 orbitals. Because this corresponds to a MC transition, the d orbitals are no longer oriented according to the Cartesian coordinates of the two pz rings.

The DFT calculations indicate that the two metals in the lowest-energy ^{3}MLCT excited state of *trans,trans*-$[\{Ru(NH_3)_4(py)\}_2(pz)]^{4+}$ have the same amount of charge (see Figure 8). Figure 8 also compares the calculated Mulliken spin densities of *trans*-$[Ru(NH_3)_4(py)(pz)]^{2+}$, *trans*-$[Ru(NH_3)_4(py)_2]^{2+}$, $[Ru(NH_3)_5(pz)]^{2+}$, and $[Ru(NH_3)_5(py)]^{2+}$ in their T_0 states. An unexpected feature of the modeled T_0 states of the monometallic complexes is that the reduced MDA rings are displaced from their ground-state planes by 30−40° in the acetonitrile solvent but not in the gas phase; the potential energy barrier for interconversion of the two equivalent out-of-plane MDA-ring displacements is small (260 cm^{-1} calculated for MDA = pz).

We have also calculated the ground-state electronic structures for two of the one-electron-oxidized complexes, and the calculated Mulliken spin densities of *trans*-$[Ru(NH_3)_4(py)(pz)]^{3+}$ and *trans,trans*-$[\{Ru(NH_3)_4(py)\}_2pz]^{5+}$ are shown in Figure 9. These calculations show that the d-orbital populations of the Ru centers are the same in the respective T_0 states and Ru^{III} complexes.

The NTOs calculated for the lowest-energy MLCT transitions, of the *trans,trans*-$[\{Ru(NH_3)_3(py)\}_2(pz)]^{4+}$ and

dx.doi.org/10.1021/ic4016614 | Inorg. Chem. 2013, 52, 9774−9790

Table 5. Comparison of the Orbital Occupations of T_0 and the Nearest-Energy ^{3}MC Excited States of *trans*-$[Ru(NH_3)_4(pz)_2]^{2+}$

	^{3}MLCT			^{3}MC-d_{xy}			^{3}MC-d_{yz}		
Energy (kcal/mol)	0			3.53			0.26		
Spin Density	Ru: 1.04			1.95			1.95		
Corresponding orbitals	α- HOMO α- HOMO-1			α- HOMO α- HOMO-1			α- HOMO α- HOMO-1		
Geometry(Å)	Ru-N (pz)	Ru-N' (pz)	Ru-N (NH_3)	Ru-N (pz)	Ru-N' (pz)	Ru-N (NH_3)	Ru-N (pz)	Ru-N' (pz)	Ru-N (NH_3)
	2.154	2.047	2.139 2.147	2.080	2.080	2.557 2.188	2.640	2.640	2.160

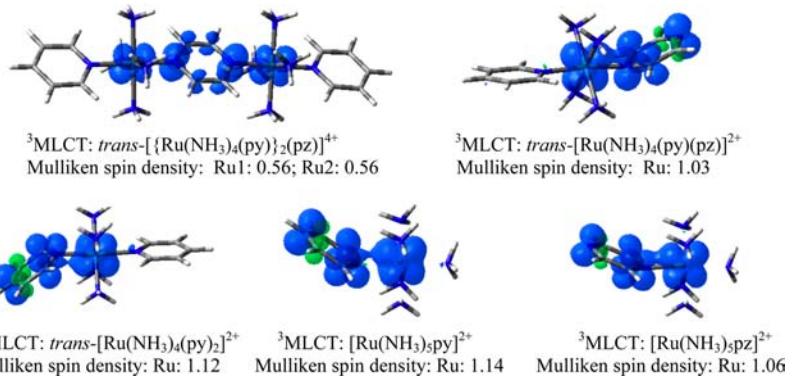

Figure 8. Comparison of the spin densities of several Ru-MDA complexes in their T_0 excited states.

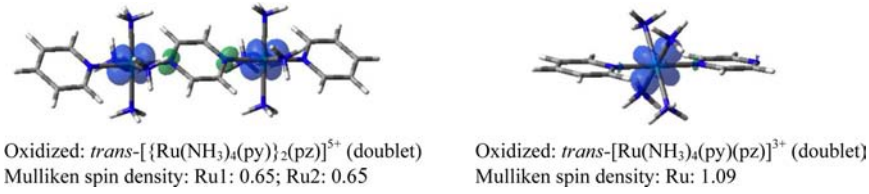

Figure 9. Comparison of the spin densities of *trans*-$[Ru(NH_3)_4(py)(pz)]^{3+}$ and *trans,trans*-$[\{Ru(NH_3)_4(py)\}_2pz]^{5+}$ in their one-electron-oxidized states.

dx.doi.org/10.1021/ic4016614 | *Inorg. Chem.* 2013, 52, 9774−9790

trans-$[Ru(NH_3)_4(py)(pz)]^{2+}$ complexes are characteristic of the Ru-pz chromophore (see Figures 10 and 11), and the 77 K emission does not have the vibronic sideband structure typical of the bpy-ligand distortions consistent with the Ru-pz chromophore. These observations indicate that the lowest-energy ^{3}MLCT excited-state energies do not differ much for the different chromophores, but everything else being equal, the excited-state energies decrease in the order Ru-bpy < Ru-pz < Ru-py.

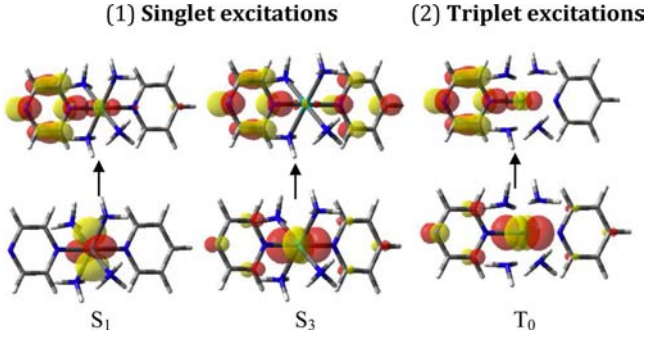

Figure 10. NTOs for the singlet and triplet excited states (TD-DFT calcualtions) with ground-state nuclear coordinates of *trans*-$[Ru(NH_3)_4(py)(pz)]^{2+}$.

DISCUSSION

We have determined the absorption spectra of a dozen simple Ru^{II}-ammine complexes with MDA ligand chromophores (where MDA = py, a substituted py, or pz). We have found that about half of these complexes emit in 77 K glasses. Our DFT modeling of the absorption spectra indicates that the dominant, observed low-energy MLCT absorption bands do not correspond to the lowest-energy MLCT excited state (S_1; a HOMO → LUMO transition) similar to our findings for the closely related Ru^{II}-bpy complexes,[20,21] but DFT modeling indicates that MLCT excited states produced by the dominant absorptions have electronic configurations that correlate with the lowest-energy ^{3}MLCT excited states, in contrast to our observations on the complexes with Ru-bpy chromophores. The observed 77 K emissions appear to be weak. We have computationally modeled the lowest-energy triplet excited states of selected complexes in order to provide further insight into the excited-state properties of this class of complexes.

A. Absorption Spectra of the Ru-MDA Complexes. Our computational modeling indicates that the dominant ambient absorption bands found for the $[Ru(L)_{6-n}(MDA)_n]^{2+}$ complexes (n = 1−3) are generally composites of several configurationally different electronic transitions and that the S_0/S_1 transitions generally occur with significantly lower energies and with oscillator strengths so small that they would be difficult to observe. The well-defined shoulder at about 17000 cm^{-1} in the 87 K spectrum of the *trans*-$[Ru(NH_3)_4(pz)_2]^{2+}$ complex (Figure 7) is consistent with the very weak S_0/S_1 transition found in the DFT modeling. This general pattern of S_0/S_1 transition energies and oscillator strengths results from modeling with both the B3PW91 and LC-wPBE functional. However, about 40% of the calculations with the LC-wPBE functional for the complexes with monodentate Ru-MDA chromophores result in a lowest-energy MC excited state, and a majority of these (about 70%) have significant 77 K emissions that are typical of the MLCT excited states. The origins of these differences are not clear at this time; nevertheless, the LC-wPBE calculations support the hypothesis that the lowest-energy MC and MLCT excited states may be close in energy. In general, both the dominant absorption maxima and the S_0/S_1 transition energies calculated using the B3PW91 functional do correlate well with the differences in the calculated potentials for the first oxidations and first reductions

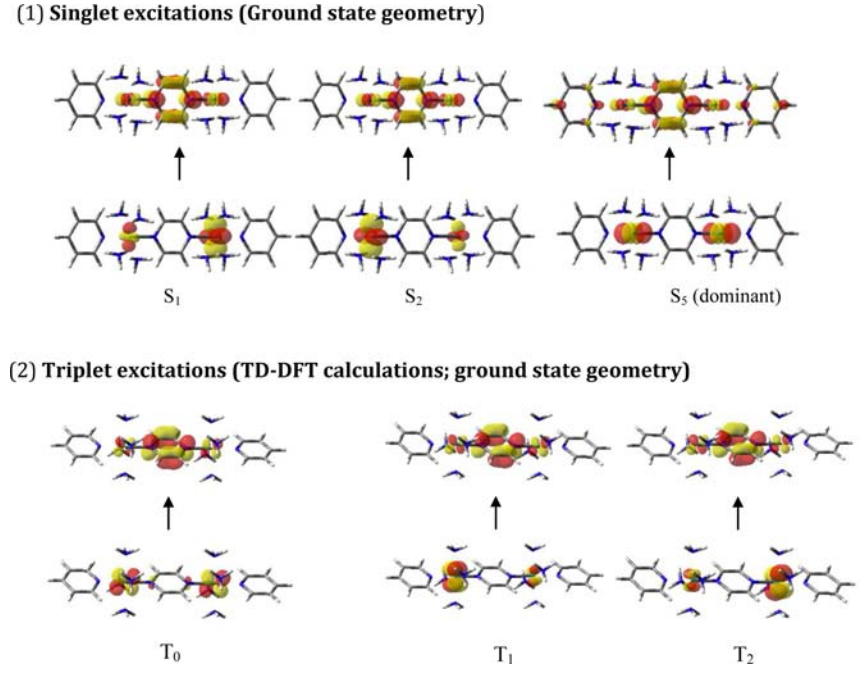

Figure 11. NTOs for lowest-energy ^{1}MLCT excited states and for the T_0 excited state of **13**. The lowest-energy ^{1}MLCT excited state with significant oscillator strength is S_5. Note that while S_1 and S_2 have very similar energies and correspond to a localized (Ru^{III}/Ru^{II}) Franck−Condon excited-state structure, the two Ru centers of T_0 have similar electronic populations.

dx.doi.org/10.1021/ic4016614 | *Inorg. Chem.* 2013, 52, 9774−9790

of the complexes, and the complexes with Ru-MDA chromophores are indistinguishable from the complexes with Ru-bpy chromophores in this correlation (Figure 12). If one

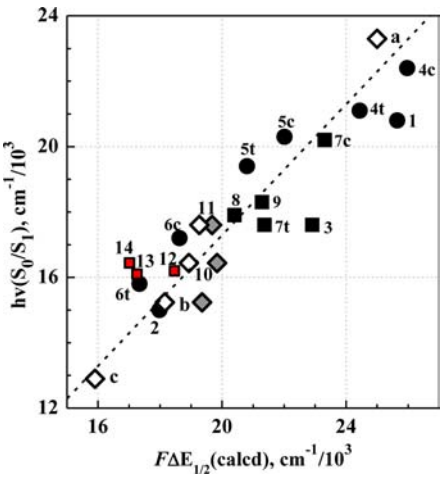

Figure 12. Comparison of the calculated S_0/S_1 transition energies to the differences in potentials for oxidation and reduction of the complexes: filled symbols for calculated potentials; open diamonds for experimental potentials; squares for Ru-pz chromophores, black for monoruthenium complexes, and red for diruthenium complexes; circles for Ru-Y-py chromophores; diamonds for Ru-bpy chromophores. The dashed line is drawn with a slope of 1.00 and an intercept of −2700 cm^{-1}. The complexes corresponding to the numerical and letter designations are identified in Tables 1−3.

assumes, as is often stated, that the first oxidation and first reduction of the complex probe the HOMO and LUMO, respectively, then $F\Delta E_{1/2} > h\nu(S_0/S_1)$ could be related to the differences in the solvent contributions to the optical transitions and electrochemical processes, ΔG_{solv}, as in eq 3.[9,10,80,81]

$$h\nu_{max}(\text{abs};\ S_0/S_1) \approx F\Delta E_{1/2} + \lambda_e + \Delta G_{solv} \quad (3)$$

However, this interpretation requires that $|\Delta G_{solv}|$ must be larger than the nuclear reorganizational energy for the vertical transition, λ_e. Variations in $\lambda_e + \Delta G_{solv}$ from one complex to another could contribute to the scatter in Figure 12, but it seems unlikely that this quantity is the same in the Ru-bpy and Ru-MDA complexes. Another interpretation of $F\Delta E_{1/2} > h\nu(S_0/S_1)$ is that the d-orbital electronic configuration of the oxidized complexes does not always correlate with that of S_1. The latter appears to be the case for some of the Ru-MDA complexes, and this is discussed in the next section.

B. Emission Spectra of the Ru-MDA Complexes. *1. General Features of the Emitting States.* The calculated reduction potentials suggest that reduction of the coordinated pz or Y-py ligands occurs at potentials that are several hundred millivolts more negative than those of coordinated bpy. This is in agreement with (a) our inability to find the MDA ligand reductions and (b) the observation that the emission of complex **11** is typical of the Ru-bpy chromophore, while that of **9** is typical of the Ru-pz chromophore. Thus, the Ru-MDA MLCT excited states tend to have higher energies than those observed for the MLCT excited states with a Ru-bpy chromophore if everything else is equal.

The lack of distinguishable vibronic features in the emission spectra that can be attributed to MDA ligand (MDA = pz or Y-py) distortions of the Ru-MDA chromophores contrasts with the emission spectra of the Ru-bpy chromophores, which are similar in energy, and this is surprising because one might expect that an electron localized on a single pz or Y-py ring will result in larger amplitude distortions than an electron distributed over the two py rings of bpy. Possible origins of this contrast in relative vibronic sideband amplitudes are (a) more ground-state/excited-state electron delocalization in Ru^{II}-MDA than Ru^{II}-bpy complexes, (b) more metal−ligand distortion in Ru-MDA than in the Ru-bpy complexes, and/or (c) because a large amount of the MLCT excited-state distortion of the bpy ligand is in the C1−C1′ linkage between pyridyl rings and the vibronic contributions are proportional to the squares of the distortions in the individual vibrational modes,[21] the differences in the distributions of distortions over the aromatic ring vibrational modes may also contribute.

The excited-state distortion parameters that have been inferred from the resonance Raman (rR) spectra of $[Ru(NH_3)_4bpy]^{2+}$[15] and *trans*-$[Ru(NH_3)_4(ac\text{-}py)_2]^{2+}$ [21,36] imply that the vibronic sideband amplitudes of the latter make a larger fractional contribution to the emission spectrum than do those of the former (Supporting Information Table S4 and Figure S4).[45] The rR data suggest that the relative contributions of the squared distortions of the aromatic rings to the emission spectra should be roughly comparable (in significant part because of the contributions of the C1−C1′ distortions) for the two complexes, and the similarity of the energies of the aromatic ligand distortions is supported by the DFT-calculated distortion energies of 1600, 1500, and 1600 cm^{-1} for the py, pz, and bpy ligands, respectively, in the corresponding MLCT excited states. However, our computational modeling indicates that there are more distortions in low-frequency modes of the $[Ru(NH_3)_4bpy]^{2+}$ complex than suggested by the reported rR parameters,[21] and the implied insensitivity of rR spectra to some low-frequency modes complicates these comparisons. Overall, the rR parameters are consistent with the observed differences in the $[Ru(NH_3)_4bpy]^{2+}$[15] and *trans*-$[Ru(NH_3)_4(ac\text{-}py)_2]^{2+}$ emission spectra (see Supporting Information Figure S4B).[45]

There should be nearly a 1:1 correspondence between the absorption and emission energy maxima for electronic transitions that differ only in spin multiplicity. In an idealized limit in which the contributions of the stabilization energies that result from configurational mixing (ε_x; x = S, singlet, or T, triplet) are very small compared to the energy differences between the diabatic states, the energies of the respective maxima can be parametrized with respect to the difference in metal and acceptor-ligand reduction potentials ($\Delta E_{1/2}$),[9,10,80,81]

$$h\nu_{max}(\text{emis}) \approx F\Delta E_{1/2} - \lambda_g - E_{ST} - \Delta G_{solv} \quad (4)$$

where λ_g is the reorganizational energy associated with the vertical relaxation of the excited state and E_{ST} is the energy difference between the CT excited states with singlet (S) and triplet (T) spin multiplicity but the same orbital occupation. When λ_g, λ_e, and E_{ST} are approximately constant through a series of complexes, a 1:1 correspondence of $h\nu_{max}(\text{abs};\ S_0/S_1)$ and the observed emission maxima $h\nu_{max}(\text{emis})$ should result. This is very nearly the case for the calculated (B3PW91) vertical $S_0 \rightarrow S_1$ transitions of the monometallic complexes considered here, as is illustrated in Figure 13.

Within reasonable uncertainties, the emission energy maxima of the monometallic Ru-MDA complexes track their absorption maxima. Our computational modeling of the complexes with Ru-bpy chromophores has indicated that the electronic configuration of T_0 correlates with that of S_1 and not with

dx.doi.org/10.1021/ic4016614 | Inorg. Chem. 2013, 52, 9774−9790

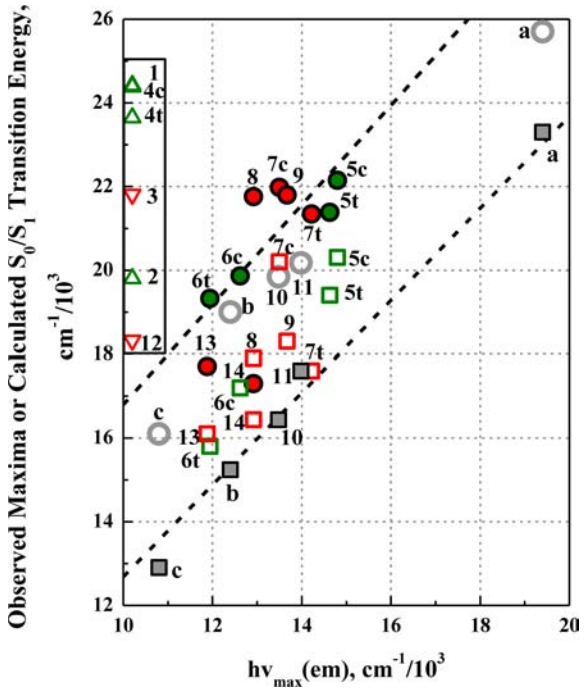

Figure 13. Correlation of the observed absorption maxima (circles) and calculated (B3PW91) S_0/S_1 (squares) transition energies with the 77 K emission maxima for Ru-MDA and Ru-bpy chromophores (gray). The Ru-MDA chromophores are as follows: Ru-Y-py, green; Ru-pz, red. The filled symbols indicate whether the computationally modeled electronic configuration of T_0 for the complex correlates with the dominant electronic transition (upper) or S_0/S_1 (lower). The triangles in the box at the left are for the observed absorption maxima of complexes whose emission was not detected in this study. The dashed lines are fitted to the Ru-bpy (lower) and Ru-MDA (upper) chromophores and have slopes of about 1.1 and 1.2, respectively, and intercepts that differ by about 4000 cm^{-1}.

the dominant, observed absorption band;[20,21] consequently, the energies calculated for S_1 are a useful upper limit on the T_0 energies in Ru-bpy complexes, and the energy differences between the S_1 and T_0 minima are less than 3000 cm^{-1}.[21] This is not the case for the complexes with Ru-MDA chromophores. For these complexes, the electronic configurations of the dominant low-energy absorption band, corresponding to the lowest-energy calculated transition with significant oscillator strength, correlate with the electronic configurations of the lowest-energy ^{3}MLCT excited state for the complexes examined here, and the difference between $hν_{max}$(abs) and $hν_{max}$(emis) is about 7000 cm^{-1}.

For the absorption bands assigned as indicated by the computational modeling and based on eqs 1 and 2, the quantity $(λ_g + λ_e + E_{ST} + 2ΔG_{solv})$ is about 4000 cm^{-1} larger for Ru-MDA than for the Ru-bpy chromophores. The Ru d-orbital configurations are different in the T_0 states of the two classes of chromophores (approximately d_{yz} and d_{xy}, respectively), and some of this difference appears to arise from the excited-state distortions $(λ_g + λ_e)$, which are significantly larger for the Ru-MDA systems, as discussed above, and some may arise from differences in the exchange energy (contributing to E_{ST}). Both contributions are likely related to the greater dπ/pπ spatial overlap in the Ru-MDA systems.

An important feature of Figure 13 is that either the observed absorption maxima or the calculated S_0/S_1 transition energies for the $[Ru(NH_3)_{6-n}(MDA)_n]^{2+}$ complexes are within the range of those for emitting monobipyridine complexes (see Table 2) and that there is no simple pattern of energies that distinguishes the Ru-MDA complexes for which we find well-defined emissions and those whose emissions we have not been able to detect. The difficulty in detecting an emission could be the result of either a very short excited-state lifetime or a very small radiative yield. It would be difficult to detect excited-state emissions whose lifetimes were much less than about 5 ns with our instrumentation.

The comparisons discussed here indicate that the bandshapes and energies of the $[Ru(NH_3)_{6-n}(MDA)_n]^{2+}$ emission spectra have the characteristics that one expects of Ru-MDA ^{3}MLCT excited states. That medium-frequency vibronic sidebands are not observed in the Ru-MDA emission spectra is readily attributed to the relatively large coordination sphere distortions of their ^{3}MLCT excited states and the effects of vibronic component overlap when bandwidths are large in a system with distortions in many vibrational modes.[17] The emission energies correlate with the MLCT absorption energies and are modeled well by the DFT calculations (Table 4). However, these complexes emit very weakly, and the comparison of their lifetimes and quantum yields suggests some unusual features in the properties of their higher energy excited states, as is discussed in the next section.

2. Excited-State Lifetimes and Emission Yields. The Franck−Condon excited states of the overwhelming majority of the transition-metal complexes examined to date relax very rapidly and efficiently to the lowest-energy excited state, and the excited-state properties that determine whether or not an emission is easily detected are the intrinsic radiative yield (or inverse radiative rate constant, k_r^{-1}) and the physical factors that alter the excited-state lifetime. As noted in the Introduction, the lifetimes of the lowest-energy excited states of these complexes are usually functions of the rate constants for nonradiative relaxation (k_{nr}), internal conversion (k_{ic}) to a different electronic excited state (in this context, probably a ^{3}MC state), or intermolecular quenching processes involving T_0 (k_q). Upper-state photochemistry has often been observed,[6−10,82−88] and low-temperature emission yields significantly less than unity are known[26,50,82,88] for transition-metal complexes. However, small low-temperature emission yields are usually related to $k_{nr} \gg k_r$, and the inefficient population of low-temperature emitting excited states of transition-metal complexes is unusual.

The quantum yield for emission can be expressed as

$$\phi_r = \eta_{CT}\frac{k_r}{k_r + k_{nr} + k_{ic} + k_q} \quad (5)$$

where η_{CT} is the efficiency of populating the emitting excited state; $\eta_{CT} \approx 1$ for most polypyridine transition-metal complexes. One expects k_r and k_{nr} to be largely functions of the chromophore,[50] while k_{ic} will depend on details of the complex's electronic structure and the barrier to internal conversion and k_q will be related to the solvent medium. While there should be some small variations in d-orbital splittings among the $[Ru(NH_3)_{6-n}(MDA)_n]^{2+}$ complexes, these are not likely to lead to very large variations in the relative energies of the potential energy minima ($E^{0'0}$) of the ^{3}MLCT and ^{3}MC excited states. A very simple limit considers that (1) $E^{0'0}(^3MC)$ is approximately constant through the series of $[Ru(NH_3)_{6-n}(MDA)_n]^{2+}$ complexes, (2) $E^{0'0}(^3MLCT)$ varies in

dx.doi.org/10.1021/ic4016614 | Inorg. Chem. 2013, 52, 9774−9790

the same manner as the observed dominant absorptions transitions, and (3) internal conversion is the dominant mechanism for ^{3}MLCT relaxation. In this limit, the $E^{0'0}(^3\text{MLCT})$ excited-state lifetimes of the $[\text{Ru}(\text{NH}_3)_{6-n}(\text{MDA})_n]^{2+}$ complexes will tend to increase in the order for MDA of pz < ac-py < ph-py < py. This is not what we observe (Table 2 and Figure 15).

Figure 14 qualitatively illustrates the potential energy surfaces for the regimes of excited-state behavior expected when $\eta_{CT} \approx 1$ with (I) $E^{0'0}(^3\text{MLCT}) \gg E^{0'0}(^3\text{MC})$, (II) $E^{0'0}(^3\text{MLCT}) \approx E^{0'0}(^3\text{MC})$, and (III) $E^{0'0}(^3\text{MLCT}) < E^{0'0}(^3\text{MC})$. The calculated S_0/S_1 energies of Ru-MDA chromophores are largest for MDA = py, and we have not yet found emissions for these complexes. This suggests that they fall into the regime with $E^{0'0}(^3\text{MLCT}) > E^{0'0}(^3\text{MC})$ (part I of Figure 14), where internal conversion is probably in the sub-picosecond regime.[14,22] If $E^{0'0}(^3\text{MLCT}) < E^{0'0}(^3\text{MC})$, then the ^{3}MC state may weakly mix with the ^{3}MLCT excited state, but the emission should be reasonably typical of the class of complexes with the inverse excited-state lifetime approximately equal to the sum of the radiative and nonradiative rate constants.

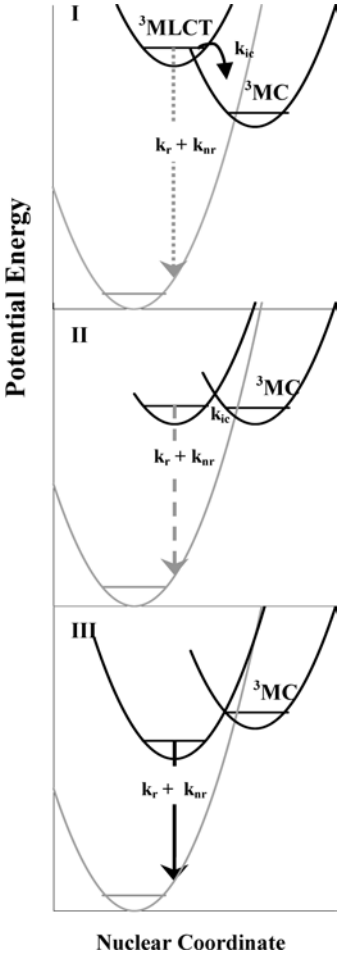

Figure 14. Qualitative potential energy diagrams illustrating the relative energies of MC and MLCT excited states in the limit that there are no complications from other excited states and the lowest-energy excited state is populated with unitary efficiency: (I) $E^{0'0}(^3\text{MLCT}) > E^{0'0}(^3\text{MC})$; (II) $E^{0'0}(^3\text{MLCT}) \sim E^{0'0}(^3\text{MC})$; (III) $E^{0'0}(^3\text{MLCT}) < E^{0'0}(^3\text{MC})$. Note that the distortion coordinates of the MC and MLCT excited states are different so the potential energy surfaces are more complicated than indicated in this diagram.

If $\eta_{CT} \approx 1$, then the excited-state lifetimes approximately distinguish the three limits in Figure 14: (I) when k_{ic} is larger than $k_r + k_{nr}$, any emission from the MLCT excited state should be very short-lived and weak ($\tau^{-1} \approx k_{ic}$); (II) the MLCT excited-state emission intensity and lifetime will be functions of the barrier for crossing between the MLCT and MC excited states and temperature-dependent ($\tau^{-1} = k_{decay} \approx k_r + k_{nr} + k_{ic}$); (III) the MLCT excited-state emission depends on the physical properties of the isolated MLCT excited state [$\tau^{-1} \approx (k_r + k_{nr})_{CT}$].

Because k_{ic} corresponds to a barrier crossing process, it will be temperature-dependent and, therefore, so will the ^{3}MLCT excited-state lifetime and emission intensity. In order for the internal conversion process to compete with $k_r + k_{nr} \approx 10^6$ s^{-1} at 77 K, the barrier heights would have to be less than about 700 cm^{-1}. This is somewhat restrictive, and some the observed emissions could be from local ^{3}MLCT minima with $k_r + k_{nr} > k_{ic}$ even when $E^{0'0}(^3\text{MC})$ is slightly lower than $E^{0'0}(^3\text{MLCT})$. There is a great deal of scatter in the observed emission decay constants, k_{decay}, in Figure 15, but there are no systematic deviations from the expectation of an exponential dependence of k_{nr} on $E^{0'0}(^3\text{MLCT})$.[23] Furthermore, if the emission were from a local minimum, one would expect relatively large contributions from k_{ic} to result in an anomalously large value of k_{decay}; such an anomalously large value of k_{decay} has been reported for [Ru(1,4,7,11-tetraathiatetradecane)bpy]$^{2+}$,[21] which does suggest that the emission observed from this complex may be from a local minimum. There is no evidence for this kind of behavior in the complexes reported here. It is to be noted that the values k_{decay} reported for an extended collection of $[\text{Ru}(\text{Am})_4\text{bpy}]^{2+}$ complexes[18] scatter similarly around the solid line in Figure 15, which is somewhat surprising because k_{nr} is expected to be a function of the nuclear displacements of the excited state,[23] and these will be different for different chromophores. Overall, the emission lifetimes found for the Ru-MDA chromophores follow closely the pattern expected for $\tau^{-1} \approx (k_r + k_{nr})_{CT}$.

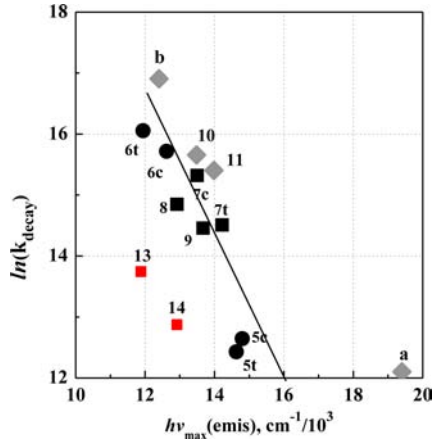

Figure 15. Correlation between the 77 K decay rate constants and the emission maxima. See Table 2 for the identity of the complexes.

The apparently anomalously long lifetime for the $[\text{Ru}(\text{CH}_3\text{CN})_4\text{bpy}]^{2+}$ complex ("a" in Figure 15) compared to the

dx.doi.org/10.1021/ic4016614 | Inorg. Chem. 2013, 52, 9774−9790

Table 6. Summary of Observations on Two Closely Related Complexes[a]

approach	quantity determined	*trans*-$[Ru(NH_3)_4(pz)_2]^{2+}$	*trans*-$[Ru(NH_3)_4(pz)(py)]^{2+}$	$[Ru(bpy)_3]^{2+}$ [for perspective]
experimental	absorption max (300 K)	20.4	21.1	22.2
	absorption max (87 K)	19.2 (16.9, sh)	19.7 (16.9, sh)	22.1 (18.8, sh)
computational	E(dominant)[b]	21.5	22.6	
		$d_{yz} \rightarrow$ pz(LUMO)	$d_{yz} \rightarrow$ pz(LUMO)	
	$E(S_0/S_1)$[b]	17.7	17.9	
		$d_{xy} \rightarrow$ pz(LUMO)	$d_{xy} \rightarrow$ pz(LUMO)	
experimental	emission max (77 K)[c]	12.9 (14.2)	12.3 (12.9)	17.2
	emission lifetime (77 K),[c] ns	50 (500)	76 (300)	7700
	emission quantum yield (77 K)[c]	~0.00005 (0.002)	~0.00004 (0.0003)	0.38[d]
computational	ΔE for lowest-energy ^{3}MLCT (T_0)[e]	11.4	10.4	
		$d_{yz} \rightarrow$ pz(LUMO)	$d_{yz} \rightarrow$ pz(LUMO)	
	ΔE for lowest-energy ^{3}MC states[f]	11.5	10.8	
		12.6	12.7	

[a]All experimental and computational spectra in energies as $\times 10^3$ cm^{-1}; experimental emission/absorption energy in ethanol/methanol; calculated energies in acetonitrile using PCM solvation. [b]Vertical excitation energies computed by TD-DFT using the S_0-optimized geometry, along with the approximate orbital transitions based on an NTO analysis. [c]Ethanol/methanol glass (butyronitrile glass). [d]Reference 50. [e]Vertical emission energies computed by ΔS_{CF} using the T_0 SCF-optimized geometry and S_0 computed at the T_0 geometry, along with the approximate orbital transitions based on a corresponding orbital analysis. [f]Emission energies computed by ΔS_{CF} using the ^{3}MC SCF-optimized geometries and S_0 computed at the T_0 geometry.

$[Ru(NH_3)_{6-n}(MDA)_n]^{2+}$ complexes may arise from $k_r > k_{nr}$ for this complex in contrast to $k_r \leq k_{nr}$ for most of the complexes considered; that is, because k_{nr} is expected to decrease exponentially with excited-state energy,[23] there will be some energy for which k_r becomes greater than k_{nr}.

The emission yields determined for the *trans*-$[Ru(NH_3)_4(pz)_2]^{2+}$ and *trans*-$[Ru(NH_3)_4(pz)(py)]^{2+}$ are in the range of 10^{-5}–10^{-4}, while $\tau^{-1} \approx (k_r + k_{nr})_{CT}$ indicates that $\eta_{CT} \ll 1$ for these complexes and possibly for the whole class of Ru-MDA complexes. Furthermore, our computational modeling indicates that while the highly distorted, but bound ^{3}MC excited states are at relatively low energies for these two complexes, T_0 is a ^{3}MLCT excited state and $[E^{0'0}(^3\text{MC}) - E^{0'0}(^3\text{MLCT})] > 2k_BT_{77K}$ so that with the barrier for internal conversion, these systems should correspond to category I above. The excited-state properties of these complexes are summarized in Table 6.

Because the higher-energy excited states of transition-metal complexes have so far been found to have very short, usually sub-picosecond lifetimes, the very small emission yields suggest that one or more of the higher-energy excited states of these complexes is in some sense "dissociative". "Dissociative" usually implies bond breaking and that is possible, but it implies that the emission intensity/spectrum will change with the irradiation time, and repeated scans show no evidence of photodecomposition in 77 K glasses; however, any bond-breaking fragments could be trapped by the glass and subsequently recombine. Ultrafast electron (to solvent) or proton (from solvent) processes might also be possible quenching mechanisms. Further studies of this behavior are in progress.

The different energy range for emission of the bimetallic complexes with Ru-pz chromophores is at least partly a result of the different electrostatic contributions when one and two metals are attached to the pz ligand, and there may be a contribution from electronic delocalization. The somewhat narrower spectral width and longer lifetimes of the pz-bridged bimetallic than the analogous monometallic complexes may be related to their somewhat more restricted low-frequency Ru-pz torsional motions (see Figure 8) or possibly to electronic delocalization in the excited state. Both effects would lead to smaller excited-state distortions in the diruthenium than in the monoruthenium complexes. However, it should be noted that excited-state electronic delocalization would not be effectively mediated by a partly occupied bridging ligand orbital, and a delocalization mechanism is more likely based on "hole transfer" (mediated by ligand-to-metal higher-energy excited states) than by the electron-transfer mechanisms more typical of ground-state electronic delocalization in these complexes.[89,90] A more adequate treatment of the excited states of these multimetallic complexes requires additional experimental and computational information and is beyond the scope of this report.

CONCLUSIONS

Several Ru^{II}-ammine complexes with at least two aromatic ligands and Ru-MDA chromophores have been found to emit weakly in 77 K glasses and to have MLCT excited-state lifetimes that are comparable to those of their more strongly emitting $[Ru(L)_4bpy]^{m+}$ analogues. That the lifetimes of the Ru-MDA $^3MLCT_{(T_0)}$ states are comparable to those of the Ru-bpy chromophores with similar energies indicates that these states are relatively isolated at 77 K and that the intrinsic T_0 excited-state relaxation properties are not significantly altered by proximity to a ^{3}MC state (i.e., $k_{ic} \ll k_{nr}$). Computational modeling of the triplet states supports this interpretation because it indicates that the ^{3}MC excited-state energy minima are more than about $2k_BT$ greater than the ^{3}MLCT minima (Table 6). That the Ru-MDA $^3MLCT_{(T_0)}$ states are far weaker than those of Ru-bpy chromophores indicates that the emitting states of the former are populated much less efficiently ($\eta_{CT} \ll 1$). This implies somewhat unusual excited-state behavior in these complexes, and the computational modeling provides some clues as to how this might come about.

DFT calculations indicate that the electronic states involved in the absorption and emission maxima of Ru-MDA chromophores have similar configurations. This is in distinct contrast to our observations on complexes with Ru-bpy chromophores for which the dominant absorption and T_0 correspond to different electronic configurations.[1,2] This contrast is illustrated in Figure 16.

dx.doi.org/10.1021/ic4016614 | Inorg. Chem. 2013, 52, 9774–9790

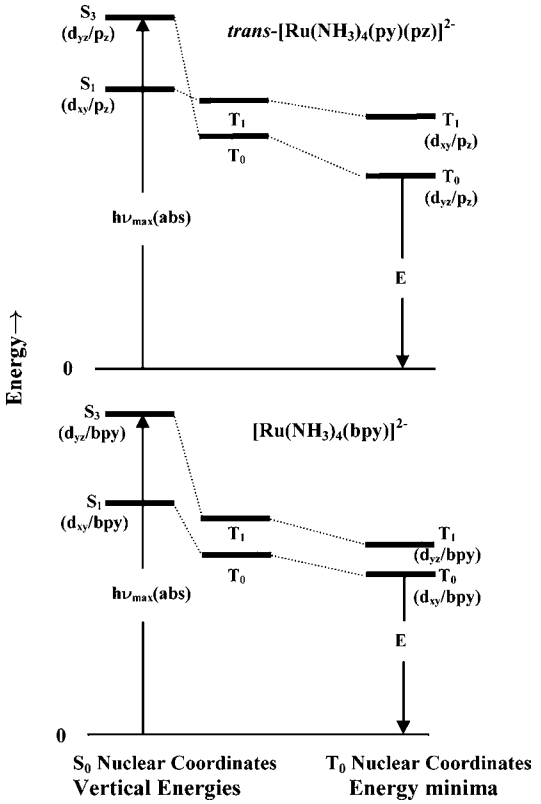

Figure 16. Qualitative representation of the contrast in the lowest-energy excited states of the Ru-MDA and Ru-bpy chromophores. The energies of states designated in the two columns on the left were calculated using nuclear coordinates of the ground-state energy minimum; those in the column on the right are for the difference in energy of the S_0 minimum and T_0 or T_1 minima (see Table 6).

This study has found some some important points about the contrasts in behavior of the Ru-MDA and Ru-bpy excited states:

1. As shown in Figure 16, the contrasting electronic configurations found for T_0 in the two classes of complexes appear to be a consequence of variations in the singlet and triplet excited-state energies, E_{ST}, for the d_{yz}/acceptor and d_{xy}/acceptor electronic configurations. For the example shown in the figure, E_{ST} is relatively large for the states with d_{yz}/acceptor configurations, and it is mostly the smaller value of E_{ST} for the d_{xy}/pz configuration of *trans*-$[Ru(NH_3)_4(py)(pz)]^{2+}$ that results in T_0 having the d_{yz}/acceptor configuration, while T_0 for $[Ru(NH_3)_4(bpy)]^{2+}$ has the d_{xy}/acceptor configuration. This is almost certainly a consequence of the differences in donor/acceptor orbital spatial overlap in these complexes in which the planes of the aromatic acceptor ligands are very different with respect to the Cartesian axes of the Ru-coordination sphere (note that the exchange integral contribution to E_{ST} is expected to increase with spatial overlap).[3]

2. There are more crossings of low-energy states in Figure 16 and therefore more mixing between these states for *trans*-$[Ru(NH_3)_4(py)(pz)]^{2+}$ than for $[Ru(NH_3)_4(bpy)]^{2+}$.

3. The metal coordination spheres of the Ru-MDA complex excited states are highly distorted, with especially large distortions involving the Ru-MDA moiety. Even at the T_0 energy minimum, the Ru−MDA bond is appreciably lengthened [0.1 Å for Ru−N(pz) compared to 0.006 Å for Ru−N(bpy) in $[Ru(NH_3)_4bpy]^{2+}]^2$ and the MDA ring is displaced from the position along the Ru−N bonding axis.

4. Preliminary determinations of the Ru-MDA emission yields indicate that the efficiencies of populating their T_0 excited states are probably less than 1%. Computational modeling of the triplet states indicates that the lowest-energy states are MLCT in nature with slightly higher-energy MC states. However, the excited-state lifetimes are not significantly different from those of Ru-bpy complexes with the same energies. This strongly suggests that T_0 is populated very inefficiently and that this inefficiency arises from very efficient upper excited-state chemistry and/or relaxation to the ground state (since these appear to be highly distorted excited states).

■ ASSOCIATED CONTENT

Supporting Information

Structures and abbreviations of complexes, emission spectra, table of electrochemistry, absorption, and 77 K emission spectra, electrochemical plots, mixed-valence absorption changes for the sample of diruthenium complexes, table of mixed-valence properties, comparison of observed and calculated absorption spectra, table of calculated state energies and NTOs, vibronic sidebands inferred from the rR parameters, and experimental details. This material is available free of charge via the Internet at http://pubs.acs.org.

■ AUTHOR INFORMATION

Corresponding Author

*E-mail: 054971@mail.fju.edu.tw (Y.J.C.), jfe@chem.wayne.edu (J.F.E.), hbs@chem.wayne.edu (H.B.S.).

Author Contributions

The manuscript was written through contributions of all authors.

Notes

The authors declare no competing financial interest.

■ ACKNOWLEDGMENTS

This work was funded in part (Y.J.C.) by the National Science Council of the Republic of China through Grant NSC 99-2113-M-030-002 and MOE Funding Direction Regarding the Development Plan for Universities and Colleges of the Republic of China and in part (J.F.E. and H.B.S.) by the Division of Chemical Sciences, Geosciences, and Biosciences, Office of Basic Energy Sciences, of the U.S. Department of Energy through Grants DE-FG02-09ER16120 and DE-SC0001907.

■ REFERENCES

(1) Crosby, G. A. *Acc. Chem. Res.* **1975**, *8*, 231.
(2) Juris, A.; Balzani, V.; Barigelletti, F.; Compagna, S.; Belser, P. L.; von Zelewsky, A. *Coord. Chem. Rev.* **1988**, *84*, 85.
(3) Kalyanasundaram, K. *Photochemistry of Polypyridine and Porphyrin Complexes*; Academic Press: New York, 1992.
(4) Balzani, V.; Credi, A.; Venturi, M. *Coord. Chem. Rev.* **1998**, *171*, 3.
(5) Balzani, V.; Juris, A.; Venturi, M.; Campagna, S.; Serroni, S. *Chem. Rev.* **1996**, *96*, 759.
(6) Ford, P. C. In *Inorganic and Organometallic Photochemistry*; Wrighton, M. S., Ed.; American Chemical Society: Washington, DC, 1978; Vol. *168*, p 73.
(7) Malouf, G.; Ford, P. C. *J. Am. Chem. Soc.* **1977**, *99*, 7213.
(8) Wagenknecht, P. S.; Ford, P. C. *Coord. Chem. Rev.* **2011**, *255*, 591.

(9) Endicott, J. F. In *Electronic Structure and Spectroscopy of Inorganic Compounds*; Solomon, E. I., Lever, A. B. P., Eds.; Wiley: New York, 1999; Vol. *2*, p 291.
(10) Endicott, J. F. In *Electron Transfer in Chemistry*; Balzani, V., Ed.; Wiley-VCH: New York, 2001; Vol. *1*, p 238.
(11) Ferraudi, G. J. *Elements of Inorganic Photochemistry*; Wiley: New York, 1988.
(12) Horvath, O.; Stevenson, K. L. *Charge Transfer Photochemistry of Coordination Complexes*; VCH: New York, 1993.
(13) Snir, O.; Weinstock, I. A. In *Physical Inorganic Chemistry: Reactions, Processes, and Applications*; Bakac, A., Ed.; John Wiley & Sons, Inc.: Hoboken, NJ, 2010, p 1.
(14) Hewitt, J. T.; Vallett, P. J.; Damrauer, N. H. *J. Phys. Chem. A* **2012**, *116*, 11536.
(15) Hupp, J. T.; Williams, R. T. *Acc. Chem. Res.* **2001**, *34*, 808.
(16) Xie, P.; Chen, Y.-J.; Endicott, J. F.; Uddin, M. J.; Seneviratne, D.; McNamara, P. G. *Inorg. Chem.* **2003**, *42*, 5040.
(17) Xie, P.; Chen, Y.-J.; Uddin, M. J.; Endicott, J. F. *J. Phys. Chem. A* **2005**, *109*, 4671.
(18) Chen, Y.-J.; Xie, P.; Heeg, M. J.; Endicott, J. F. *Inorg. Chem.* **2006**, *45*, 6282.
(19) Chen, Y.-J.; Endicott, J. F.; McNamarra, P. G. *J. Phys. Chem. A* **2007**, *111*, 6748.
(20) Allard, M. M.; Odongo, O. S.; Lee, M. M.; Chen, Y.-J.; Endicott, J. F.; Schlegel, H. B. *Inorg. Chem.* **2010**, *49*, 6840.
(21) Lord, R. L.; Allard, M. M.; Thomas, R. A.; Odongo, O. S.; Schlegel, H. B.; Chen, Y.-J.; Endicott, J. F. *Inorg. Chem.* **2013**, *52*, 1185.
(22) McCusker, J. K. *Acc. Chem. Res.* **2003**, *36*, 876.
(23) Englman, R.; Jortner, J. *Mol. Phys.* **1970**, *18*, 145.
(24) Freed, K. F.; Jortner, J. *J. Chem. Phys.* **1970**, *52*, 6272.
(25) Oesterman, T.; Abrahamsson, M.; Becker, H.-C.; Hammarstroem, L.; Persson, P. *J. Phys. Chem. A* **2012**, 1041.
(26) Yersin, H.; Braun, D.; Hensler, G.; Galhuber, E. In *Vibronic Processes in Inorganic Chemistry*; Flint, C. D., Ed.; Kluwer: Dordrecht, The Netherlands, 1989; p 195.
(27) Abrahamsson, M.; Becker, H.-C.; Hammarstrolm, L.; Bonnefous, C.; Chamchoumis, C.; Thummel, R. P. *Inorg. Chem.* **2007**, *46*, 10354.
(28) Rosokha, S. V.; Kochi, J. K. *Acc. Chem. Res.* **2008**, *41*, 641.
(29) Chen, Y.-J.; Xie, P.; Endicott, J. F. *J. Phys. Chem. A* **2004**, *108*, 5041.
(30) Chen, Y.-J.; Xie, P.; Endicott, J. F.; Odongo, O. S. *J. Phys. Chem. A* **2006**, *110*, 7970.
(31) Gould, I. R.; Noukakis, D.; Gomez-Jahn, L.; Young, R. H.; Goodman, J. L.; Farid, S. *Chem. Phys.* **1993**, *176*, 439.
(32) Odongo, O. S.; Endicott, J. F. *Inorg. Chem.* **2009**, *48*, 2818.
(33) Odongo, O. S.; Heeg, M. J.; Chen, J. Y.; Xie, P.; Endicott, J. F. *Inorg. Chem.* **2008**, *47*, 7493.
(34) Maruszewski, K.; Bajdor, K.; Strommen, D. P.; Kincaid, J. R. *J. Phys. Chem.* **1995**, *99*, 6286.
(35) Thompson, D. G.; Schoonover, J. R.; Timpson, C. J.; Meyer, T. J. *J. Phys. Chem. A* **2003**, *107*, 10250.
(36) Plummer, E. A.; Zink, J. I. *Inorg. Chem.* **2006**, *45*, 6556.
(37) Chang, J. P.; Fung, E. Y.; Curtis, J. C. *Inorg. Chem.* **1986**, *25*, 4233.
(38) Krentzien, H. J., Stanford University, Stanford, CA, 1976.
(39) Gaunder, R. G.; Taube, H. *Inorg. Chem.* **1970**, *9*, 2627.
(40) Creutz, C.; Taube, H. *J. Am. Chem. Soc.* **1969**, *91*, 3988.
(41) Creutz, C.; Taube, H. *J. Am. Chem. Soc.* **1973**, *95*, 1086.
(42) Pavanin, L. A.; da Rocha, Z. N.; Giesbrecht, E.; Tfouni, E. *Inorg. Chem.* **1991**, *30*, 2185.
(43) Zwickel, A. M.; Creutz, C. *Inorg. Chem.* **1971**, *10*, 2359.
(44) Tfouni, E.; Ford, P. C. *Inorg. Chem.* **1980**, *19*, 72.
(45) See the Supporting Information.
(46) Roberts, J. A.; Hupp, J. T. *Inorg. Chem.* **1992**, *31*, 157.
(47) Lin, J.-L.; Tsai, C.-N.; Huang, S.-Y.; Endicott, J. F.; Chen, Y.-J.; Chen, H.-Y. *Inorg. Chem.* **2011**, *50*, 8274.
(48) Drago, R. S. *Physical Methods for Chemists*; Saunders College Publishing: Philadelphia, PA, 1992.
(49) Lacky, D. E.; Pankuch, B. J.; Crosby, G. A. *J. Phys. Chem.* **1980**, *84*, 2068.
(50) Demas, J. N.; Crosby, G. A. *J. Am. Chem. Soc.* **1971**, *93*, 2841.
(51) Parr, R. G.; Yang, W. *Density-functional theory of atoms and molecules*; Oxford University Press: New York, 1989.
(52) Frisch, M. J. T.; Trucks, G. W.; Schlegel, H. B. et al.; *Gaussian Development Version*, 2012 ed.; Gaussian Inc.: Wallingford, CT, 2012.
(53) Becke, A. D. *J. Chem. Phys.* **1993**, *98*, 5648.
(54) Krishnan, R. B.; Binkley, J. S.; Seeger, R.; Pople, J. A. *J. Chem. Phys.* **1980**, *72*, 650.
(55) Perdew, J. P. *Phys. Rev. B* **1986**, *33*, 8822.
(56) Perdew, J. P.; Burke, K.; Wang, Y. *Phys. Rev.* **1996**, *54*, 16533.
(57) Andrae, D.; Haussermann, U.; Dolg, M.; Stoll, H.; Preuss, H. *Theor.Chim.Acta* **1990**, *77*, 123.
(58) Dunning, T. H., Jr.; Hay, P. J. In *Modern Theoretical Chemistry*; Schaefer, H. F., III, Ed.; Plenum: New York, 1976; Vol. *3*, p 1.
(59) Igelmann, G.; Stoll, H.; Preuss, H. *Mol. Phys.* **1988**, *65*, 1321.
(60) Vydrov, O. A.; Heyd, J.; Krukau, A.; Scuseria, G. E. *J. Chem. Phys.* **2006**, *125*, 074106.
(61) Vydrov, O. A.; Scuseria, G. E.; Perdew, J. P. *J. Chem. Phys.* **2007**, *126*, 154109.
(62) Schlegel, H. B.; McDouall, J. J. In *Computational Advances in Organic Chemistry*; Ögretir, C., Csizmadia, I. G., Eds.; Kluwer Academic: Amsterdam, The Netherlands, 1991.
(63) Bauernschmitt, R.; Ahlrichs, R. *J. Chem. Phys.* **1996**, *104*, 9047.
(64) Schlegel, H. B. *J. Comput. Chem.* **1982**, *3*, 214.
(65) Miertuš, S.; Scrocco, E.; Tomasi, J. *Chem. Phys.* **1981**, *55*, 117.
(66) Scalmani, G.; Frisch, M. J. *J. Chem. Phys.* **2010**, *132*, 114110.
(67) Scalmani, G.; Frisch, M. J.; Mennucci, B.; Tomasi, J.; Cammi, R.; Barone, V. *J. Chem. Phys.* **2006**, *124*, 9410.
(68) Tomasi, J.; Mennucci, B.; Cammi, R. *Chem. Rev.* **105**, *105*, 2999.
(69) Petit, L.; Maldivi, P.; Adamo, C. *J. Chem. Theory Comput.* **2005**, *1*, 953.
(70) Runge, E.; Gross, E. K. U. *Phys. Rev. Lett.* **1984**, 52.
(71) Stratmann, R. E.; Scuseria, G. E.; Frisch, M. J. *J. Chem. Phys.* **1998**, *109*, 8218.
(72) Martin, R. L. *J. Chem. Phys.* **2003**, *118*, 4775.
(73) Dennington, R.; Keith, T.; Millam, J. M.; *GaussView*, version 5;Semichem, Inc.: Shawnee Mission, KS, 2009.
(74) Tsai, C.-N.; Allard, M. M.; Lord, R. L.; Luo, D.-W.; Chen, Y.-J.; Schlegel, H. B.; Endicott, J. F. *Inorg. Chem.* **2011**, *50*, 11965.
(75) Isse, A. A.; Gennaro, A. *J. Phys. Chem. B* **2010**, *114*, 7894.
(76) IUPAC. Calculation of electrode potentials [Online Early Access].
(77) Namazian, M.; Lin, C. Y.; Coote, M. L. *J. Chem. Theory Comput.* **2010**, *6*, 2721.
(78) Martin, R. L. *J. Chem. Phys.* **2003**, *118*, 4775.
(79) Jakubikova, E.; Chen, W.; Dattelbaum, D. M.; Rein, F. N.; Rocha, R. C.; Martin, R. L.; Batista, E. R. *Inorg. Chem.* **2009**, *48*, 10720.
(80) Dodsworth, E. S.; Lever, A. B. P. *Chem. Phys. Lett.* **1986**, *124*, 152.
(81) Brunold, T. C.; Gudel, H. U. In *Inorganic Electronic Structure and Spectroscopy*; Solomon, E. I., Lever, A. B. P., Eds.; Wiley-Interscience: New York, 1999; Vol. *1*, p 259.
(82) Irwin, G.; Kirk, A. D. *Coord. Chem. Rev.* **2001**, *211*, 25.
(83) Endicott, J. F. In *Concepts of Inorganic Photochemistry*; Adamson, A. W., Fleischauer, P. D., Eds.; Wiley Interscience: New York, 1975; p 81.
(84) Tachibana, Y.; Moser, J. E.; Graetzel, M.; Klug, D. R.; Durant, J. R. *J. Phys. Chem.* **1996**, *100*, 20056.
(85) Asbury, J. B.; Ellingson, R. J.; Ghosh, H. N.; Ferrere, S.; Nozik, A. J.; Lian, T. Q. *J. Phys. Chem. B* **1999**, *103*, 3110.
(86) Ellingson, R. J.; Asbury, J. B.; Fererre, S.; Ghosh, H. N.; Sprague, J. R.; Lian, T.; Nozik, A. J. *Z. Phys. Chem.* **1999**, *212*, 77.
(87) Meier, A.; Selmarten, D. C.; Seiemoneit, K.; Smith, B. B.; Nozik, A. J. *J. Phys. Chem. B* **1999**, *103*, 2122.
(88) Endicott, J. F.; Ramasami, T.; Tamilarasan, R.; Lessard, R. B.; Ryu, C. K.; Brubaker, G. B. *Coord. Chem. Rev.* **1987**, *77*, 1.

(89) Creutz, C.; Newton, M. D.; Sutin, N. *J. Photochem. Photobiol., A: Chem.* **1994**, *82*, 47.
(90) Crutchley, R. *Adv. Inorg. Chem.* **1994**, *41*, 273.
(91) Dexter, D. L. *J. Chem. Phys.* **1953**, *21*, 836.